1. SCIENTIFIC RESEARCH

I. CONDENSED MATTER PHYSICS

The main objectives of research in the framework of the theme involved the application of neutron scattering techniques and complementary methods to investigate the structure, dynamics and microscopic properties of nanosystems and novel materials, which are of great importance for the development of nanotechnologies in the fields of electronics, pharmacology, medicine, chemistry, modern condensed matter physics and interdisciplinary sciences.

In 2016, the greater part of experimental research was carried out on the spectrometers of the modernized IBR-2 reactor in accordance with the Topical Plan for JINR Research and International Cooperation and FLNP User Program. A number of scientific experiments were performed in neutron and synchrotron centers in Russia and abroad under the existing cooperation agreements and accepted beam time application proposals. Also, the activities on the modernization of the available spectrometers and the development of new instruments were carried out in accordance with the development program plan for the IBR-2 spectrometers. Most attention was given to the realization of the top-priority projects (creation of the final configuration of a new DN-6 diffractometer for studying microsamples and a multipurpose GRAINS reflectometer, neutron radiography and tomography facility, upgrade of the HRFD diffractometer and REFLEX reflectometer).

Within the framework of investigations under the theme the employees of the FLNP Department of Neutron Investigations of Condensed Matter (NICM) maintained broad cooperation with many scientific organizations in Russia and abroad. The cooperation, as a rule, was documented by joint protocols or agreements. In Russia, especially active collaboration was with the thematically-close organizations, such as RRC KI, PNPI, MSU, IMP UB RAS, IC RAS, INR RAS and others.

A list of the main scientific topics studied by the employees of the NICM Department includes:

- Investigation of the structure and properties of novel functional materials;
- Investigation of the structure and properties of materials under extreme conditions;
- Investigation of fundamental regularities of real-time processes in condensed matter;
- Investigation of atomic dynamics of materials for nuclear power engineering;
- Computer simulation of physical and chemical properties of novel crystalline and nanostructured materials;
- Investigation of magnetic properties of layered nanostructures;
- Investigation of structural characteristics of carbon- and silicon-containing nanomaterials;
- Investigation of molecular dynamics of nanomaterials;
- Investigation of magnetic colloidal systems in bulk and at interfaces;
- Structural analysis of polymer nanodispersed materials;
- Investigation of supramolecular structure and functional characteristics of biological materials;
- Investigation of structure and properties of lipid membranes and lipid complexes;
- Investigation of texture and physical properties of Earth's rocks, minerals and engineering materials;
- Non-destructive control of internal stresses in industrial products and engineering materials;
- Introscopy of internal structure and processes in industrial products, rocks and natural heritage objects.

1. Scientific results

1.1. Structure investigations of novel oxide, intermetallic and nanostructured materials

Iron oxides play an important role in the formation of magnetic and other physical properties of the Earth, and find a wide range of technological applications. Recently, a new iron oxide, Fe_4O_5, which can presumably exist in the layers of the Earth's upper mantle, has been synthesized under the combined effect of high pressures and temperatures. A comprehensive study of its physical properties, as well as atomic and magnetic structure using neutron diffraction techniques at the IBR-2 reactor, has revealed a new type of the charge-ordering state with the formation of dimeric and trimeric electronic states in this compound. The phase transition into this state is accompanied by a sharp increase in the electrical resistance and a subsequent change in the symmetry of the magnetic order, namely from a collinear antiferromagnetic (AFM) order to a canting AFM order with a ferromagnetic (FM) component, as well as by a change in the nature of the modulation of the atomic structure, **Fig. 1-I-1** [1].

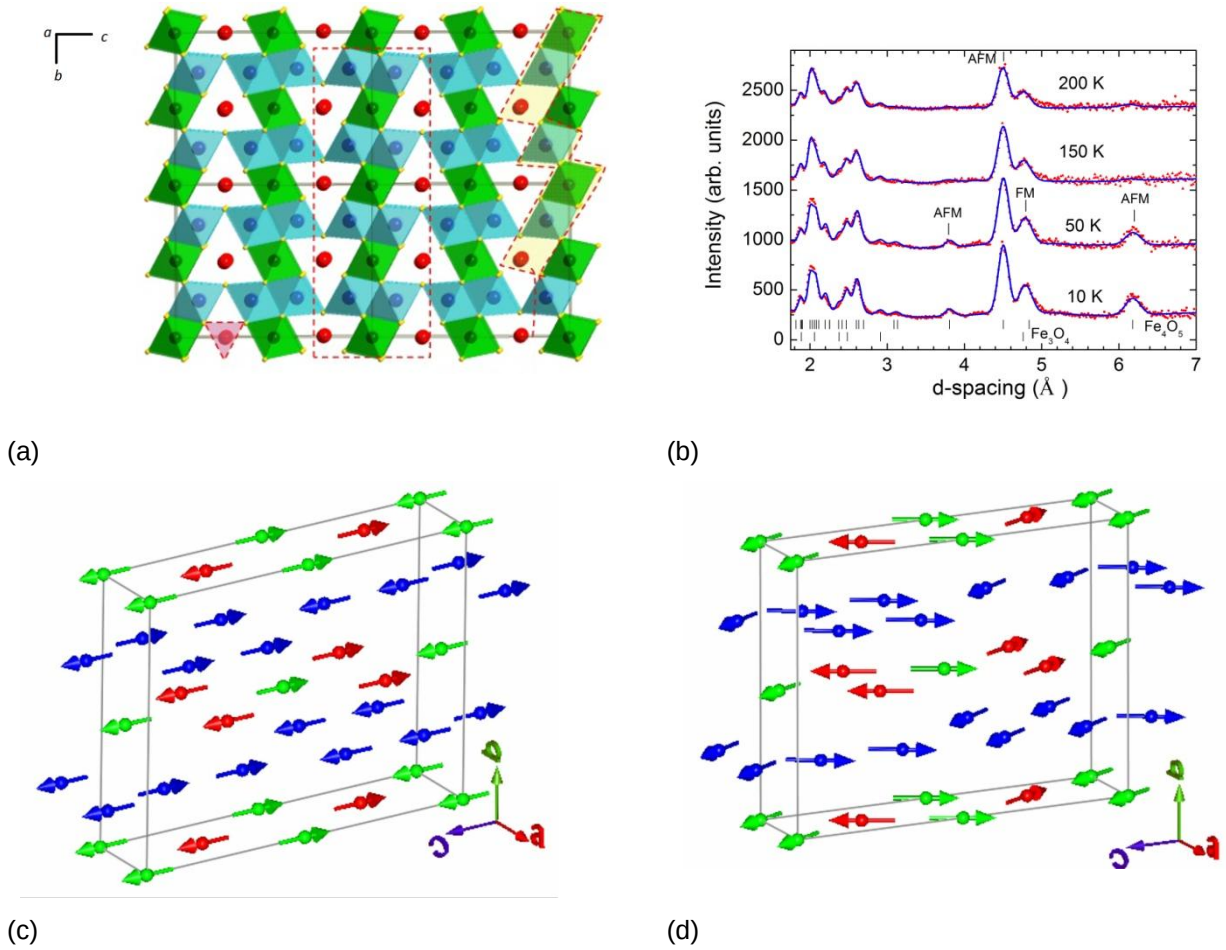

***Fig. 1-I-1**. Crystal structure of Fe_4O_5 (a), neutron diffraction spectra obtained at different temperatures and treated by the Rietveld method (b), the magnetic structure at T = 150 K (c) and T = 10 K (d).*

The search for new multiferroics and magnetoelectrics is of current interest in modern condensed matter physics and materials science. A promising system is $BaMn_{1-x}Ti_xO_3$ whose end members are a classical ferroelectric $BaTiO_3$ with a high Curie temperature (T_C = 395 K) and

1. SCIENTIFIC RESEARCH

$BaMnO_3$ – a compound exhibiting a giant magnetoelectric effect and having a relatively high temperature of magnetic ordering (T_N = 230 K). The studies of $BaMn_{1-x}Ti_xO_3$ over the entire concentration range 0 < x < 1 have revealed a very rich structural polymorphism. An increase in the titanium concentration was followed by a sequence of phase transitions between different rhombohedral and hexagonal phases differing by the ratio of oxygen octahedra connected through the corners and edges, 15R - 8H - 9R - 10H - 12R, **Fig. 1-I-2**. [2,3]. It has been found that the formation of a long-range magnetic order is possible only in structures: 9R, 8H, 15R and at concentrations of Ti $x < 0.25$, and the Neel temperature has a very sharp concentration dependence and drops from 230 to 100 K in the given *x*-range.

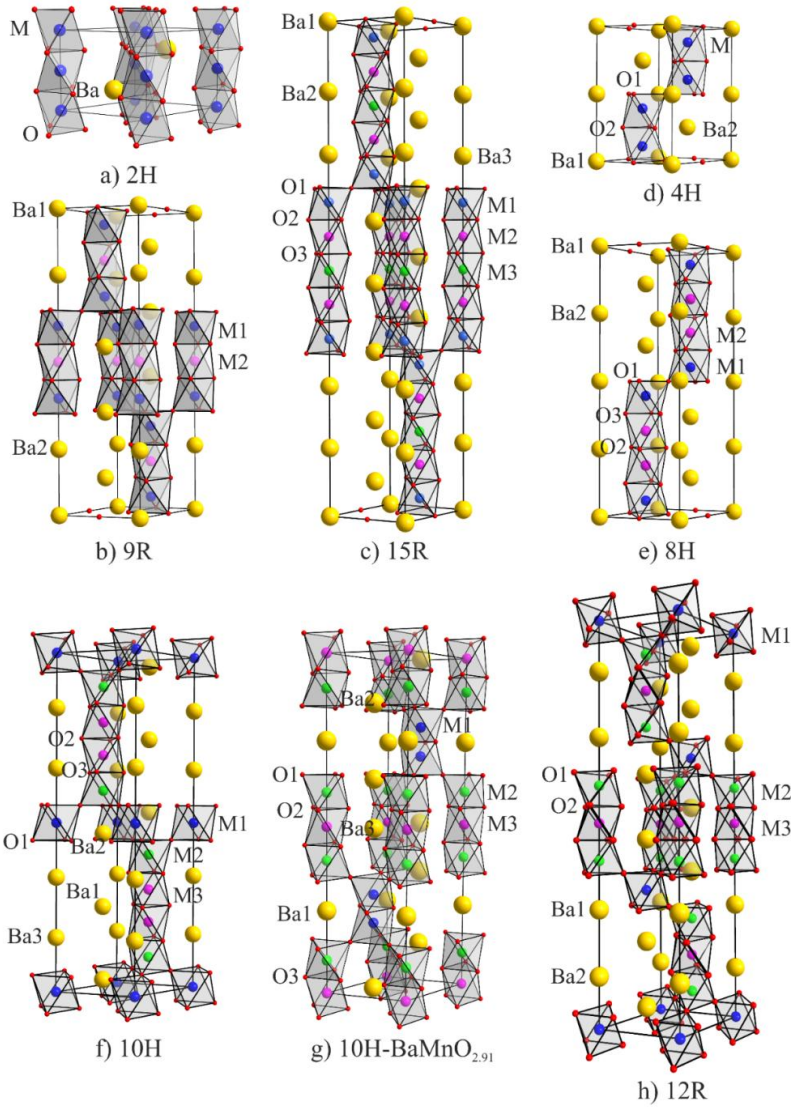

***Fig. 1-I-2**. Structure of polymorphic phases in the system $BaMn_{1-x}Ti_xO_3$.*

Using high-resolution neutron diffraction the structural (from the cubic phase to the rhombohedral phase) and magnetic (from the paramagnetic phase to the antiferromagnetic phase) phase transitions in NiO and MnO have been studied, **Fig. 1-I-3**, [4]. Despite the already long history of the study of phase transitions in simple antiferromagnets of NiO type by various experimental methods, the literature data about them are quite contradictory. It has been shown

that in MnO the structural and magnetic transitions occur simultaneously, their temperatures are the same within the experimental error: $T_{str} \approx T_{mag} \approx (119 \pm 1)$ K. For NiO the measurements were performed on powders with different mean crystallite sizes (~ 1500 nm and ~ 138 nm), and in both cases it has been found that the transition temperatures differ by ~ 50 K: $T_{str} = (471 \pm 3)$ K, $T_{mag} = (523 \pm 2)$ K.

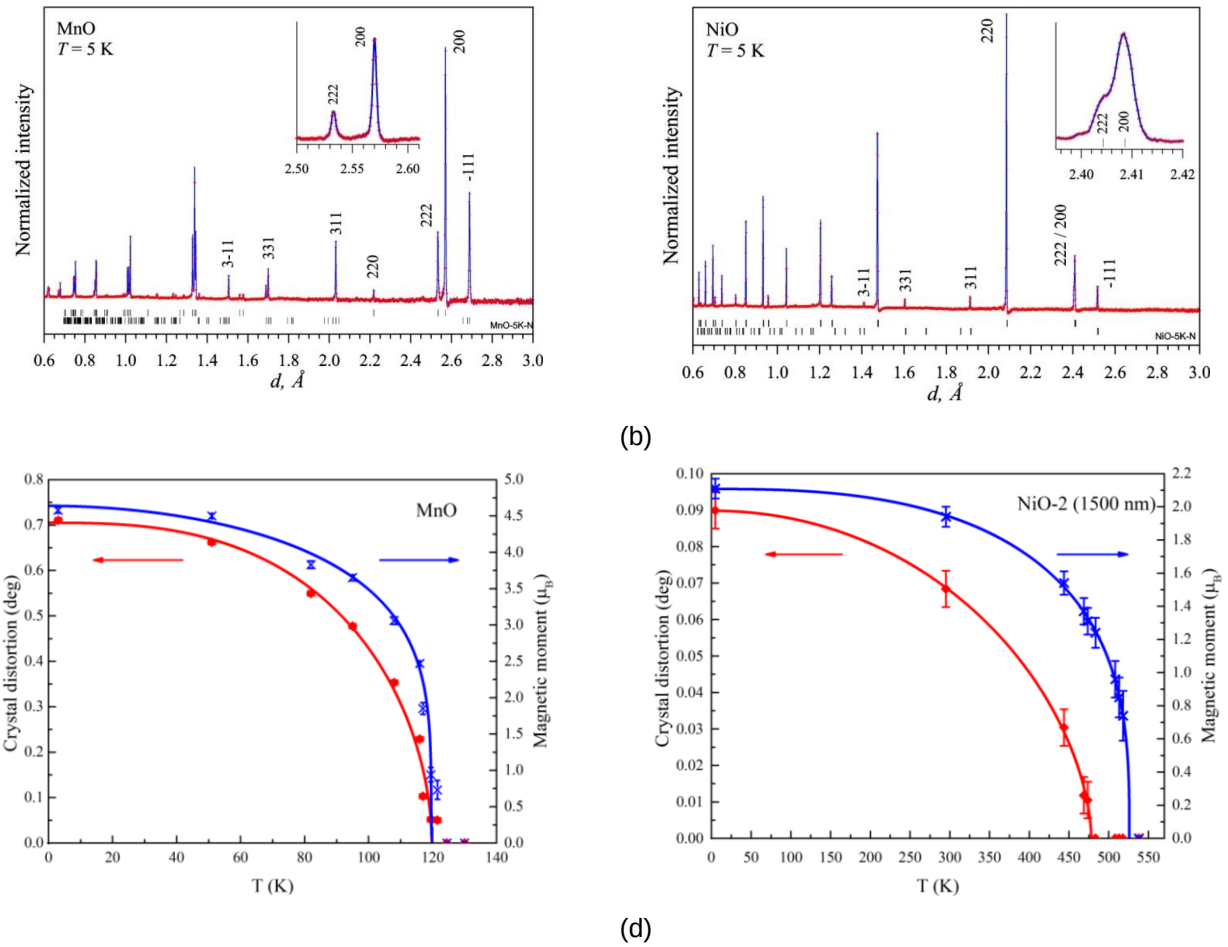

***Fig. 1-I-3**. Neutron diffraction spectra of high resolution at T = 5 K for MnO (a) and NiO (b) obtained at HRFD. Dashes indicate the positions of crystal (top row) and magnetic (bottom row) diffraction peaks. Miller indices (for a large R-lattice) are shown for several magnetic and first crystalline diffraction peaks. The inset shows the splitting of the peaks (200) and (222) due to the rhombohedral distortion. The dependence of the angle of rhombohedral distortion (left scale, red points) and magnetic moment (right scale, blue points) on temperature for MnO (c) and NiO-2 sample with the mean crystallite size of 138 nm (d).*

$La_{1-x}Sr_xFe_{2/3}Mo_{1/3}O_3$ ($0 \le x \le 1$) perovskites allow exceptionally wide variation of the Mo charge state from +3 ($x = 0$) to +6 ($x = 1$) while the charge state of Fe^{3+} remains virtually unchanged. The end members of this series show antiferromagnetic ordering in $LaFe_{2/3}Mo_{1/3}O_3$ at $T_N = 520$ K and ferrimagnetic ordering in $SrFe_{2/3}Mo_{1/3}O_3$ at $T_C = 420$ K. In both cases, the magnetic structure is dictated by antiferromagnetic superexchange between localized magnetic moments. At intermediate compositions, an interplay of antiferromagnetic-superexchange and double-exchange interactions results in nonmonotonous variations of both the magnetic-ordering temperature and saturation magnetization. To determine the magnetic phase diagram (**Fig. 1-I-4**) and the cation charge states, neutron diffraction spectra were measured, and XANES data and data on magnetic

susceptibility and magnetization were obtained. Also, the magnetic moment per formula unit was determined (**Fig. 1-I-4**). On the basis of all experimental data, a detailed analysis of the emerging interactions was carried out [5].

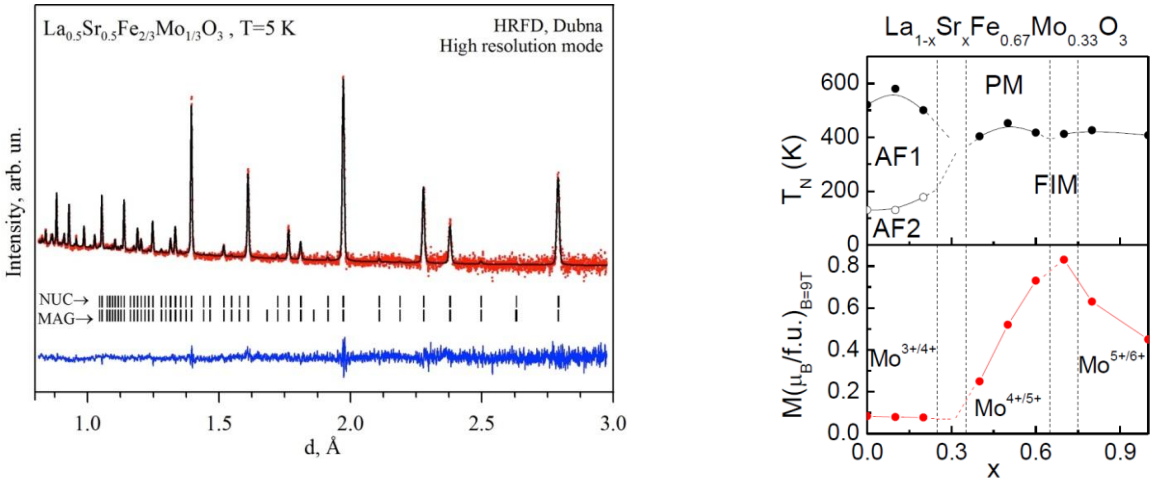

(a) (b)

***Fig. 1-I-4**. Neutron diffraction spectrum from $La_{0.5}Sr_{0.5}Fe_{2/3}Mo_{1/3}O_3$ treated by the Rietveld method (a). Experimental points, calculated function and difference curve are shown. Dashes show the calculated positions of the nuclear (top row) and magnetic (bottom row) diffraction peaks. The magnetic phase diagram (top) and the magnetic moment value measured at 2 K in a field of 9 T for the $La_{1-x}Sr_xFe_{2/3}Mo_{1/3}O_3$ series (b). Vertical lines separate the regions with different charge states of molybdenum.*

Neutron diffraction studies of the $Fe_{0.735}Al_{0.265}$ compound were carried out in a wide temperature range (20-900°C) to determine its structural states and atomic ordering mechanism [6], **Fig. 1-I-5**.

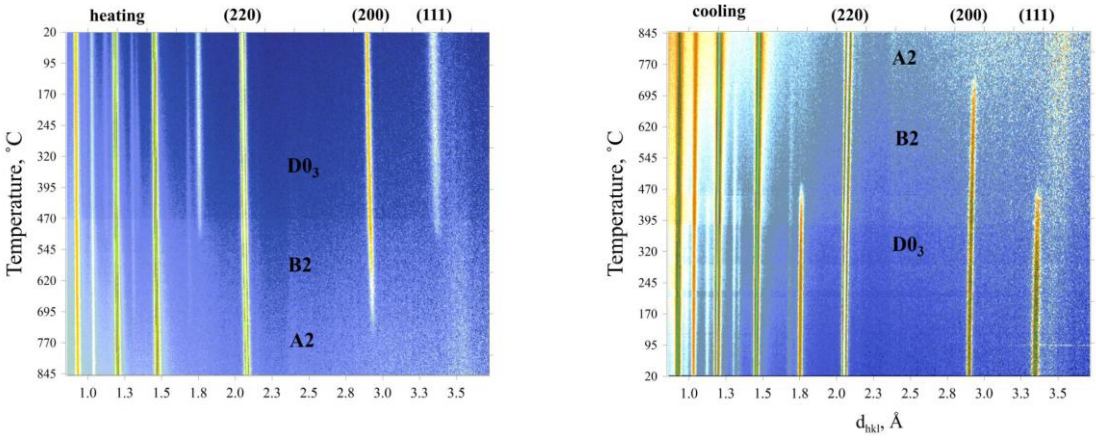

(a) (b)

***Fig. 1-I-5**. 2D representation of structural transitions in Fe-27Al under heating (a) and cooling (b). The initial (before heating) and final (after cooling) conditions – $D0_3$ phase characterized by the presence of peaks (111) and (200). In the B2 phase the peak (111) is absent, while the peak (200) remains. In the A2 phase both of these peaks are absent. The rates of heating and cooling were ±2 ℃/min, the measurement time of one spectrum – 1 min, i.e. each picture contains about 400 spectra.*

The combination of high-resolution diffraction and real-time diffraction made it possible to establish that, in contrast to traditional approaches, the structure of this compound at room temperature is a phase with only partially ordered arrangement (B2) of Fe and Al in a unit cell. A completely ordered phase (Fe_3Al - $D0_3$ type) is present as clusters of mesoscopic size (~ 200 Å) coherently incorporated into the matrix of the main phase. After the transition to a disordered state (T > 740°C) and slow cooling to room temperature, the dimensions of the structurally ordered clusters increased to ~ 900 Å.

A high contrast between the coherent neutron scattering lengths of iron and aluminum made it possible to determine with a good accuracy the temperature dependence of the occupancy factors of sites by Fe and Al atoms up to a phase transition to the disordered state. The obtained results call for further analysis of the equilibrium phase diagram for the Fe-Al system.

1.2. Investigations of magnetic fluids and nanoparticles

A number of experiments on small-angle neutron scattering (SANS) and neutron reflectometry with a horizontal sample plane for the interface of magnetic fluids with silicon (GRAINS) have been carried out in the framework of investigations of the structure and stability of magnetic nanoparticles in bulk and at interfaces, **Fig. 1-I-6** [7]. It has been found that in the bulk of aqueous ferrofluids stabilized by sodium oleate there are comparatively small (size ~ 30 nm) and compact aggregates of magnetic particles. When magnetic fluids are modified by biocompatible polymer polyethylene glycol (PEG), cluster reorganization in the bulk of magnetic fluids is observed, namely large and branched clusters (size > 130 nm, fractal dimension of 2.7) appear. The observed in-bulk reorganization of the magnetic fluids is correlated with the neutron reflectometry data, which is indicative of the formation of a single adsorption layer of magnetic particles on the surface of oxidized silicon in the initial magnetic fluid and the absence of any layer at the ferrofluid/silicon interface after the polymer modification. The study has been performed in collaboration with the Institute of Experimental Physics, Slovak Academy of Sciences (Kosice, Slovakia); the Faculty of Physics of the Taras Shevchenko Kyiv National University (Kiev, Ukraine); the National Institute of Physics and Nuclear Engineering (Bucharest, Romania); Timisoara Branch of the Romanian Academy of Sciences (Timisoara, Romania) and the Max-Planck Institute for Solid State Physics (Stuttgart, Germany).

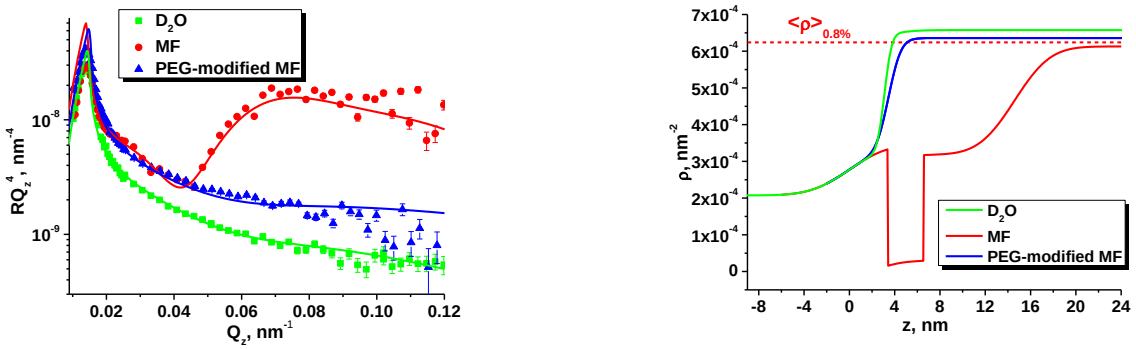

(a) (b)

***Fig. 1-I-6**. (a) Experimental reflectivity curves for heavy water and magnetic fluids; (b) resulting scattering length density profiles.*

In order to improve the synthesis procedure for biocompatible magnetic fluids, SANS (YuMO) and SAXS experiments have been carried out for magnetic fluids prepared using three

different methods (**Fig. 1-I-7**). An important feature of the ferrofluids under study was the addition of a specific component (polysaccharide agarose) to the water-based carrier, which complemented the stabilization effect and also provided biocompatibility of the initial fluids. It has been demonstrated that all investigated magnetic fluids have a complicated and highly aggregated structure, but nevertheless are stable in time. The structures of the magnetic fluids obtained by two methods of synthesis are similar to each other and different from that synthesized using the third method. In the last case two power-law type scattering levels corresponding to mass and surface fractals were observed along with an increase in the characteristic size of magnetic particles. The study [8] has been performed in collaboration with the V.I.Vernadsky Institute of General and Inorganic Chemistry (Kiev, Ukraine) and the Department of Physics of the Taras Shevchenko Kyiv National University (Kiev, Ukraine).

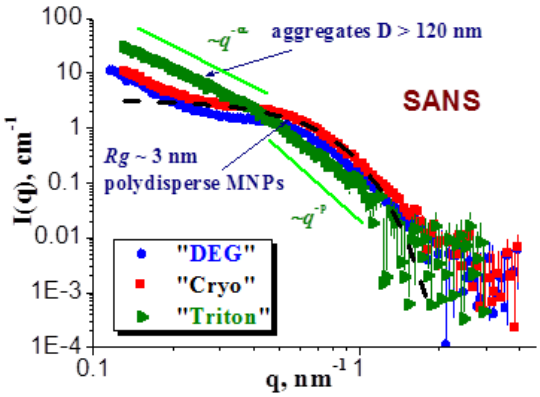

***Fig. 1-I-7**. SANS curves for magnetic fluids with agarose synthesized by three different methods. The concentration of magnetite is ~8.8. %; agarose – 0.1 vol. %.*

As a part of a comprehensive study of the interaction of magnetic nanoparticles with amyloid protein formations, the experiments on small-angle scattering of synchrotron radiation, transmission electron microscopy, atomic force microscopy and magneto-optical methods have been carried out for the mixtures of fibril amyloid aggregates of protein lysozyme (egg white) with magnetite nanoparticles in the concentration range of 0.01-0.1 vol. % [9, 10]. The analysis of the complementary data has revealed that the magnetic nanoparticles are adsorbed onto the surface of amyloids, and the adsorption mode depends on the concentration ratio between the magnetic particles and the protein in solution. Thus, with increasing concentration of magnetic nanoparticles in solution there appear particle aggregates repeating a cylindrical shape of the amyloids. The observed effect has been considered in connection with the formation of an amyloid liquid crystal phase under an external magnetic field which can be used in practice. The study has been performed in collaboration with the Institute of Experimental Physics, Slovak Academy of Sciences (Kosice, Slovakia), Department of Physics, Taras Shevchenko National University of Kyiv (Kiev, Ukraine) and Helmholtz Centre Geesthacht (Geesthacht, Germany).

In the framework of the investigation of factors affecting the stability of magnetic fluids, studies of the effect of the surfactant excess on the stability of ferrofluids have been continued [11]. In particular, using SANS the structure of magnetic fluids based on non-polar solvent decalin and stabilized by saturated monocarboxylic acids of different alkyl chain lengths (C16, palmitic acid; C12, lauric acid), with an excess of acid molecules has been studied. It has been shown that the addition of the acid to the initial stable system with an optimum composition results in structural changes associated with the more significant aggregation than that previously observed for this class of magnetic fluids. By comparing the impact of mono-carboxylic acids on the stability of non-

polar ferrofluids, one can conclude that the aggregation growth is substantially more evident in excess of palmitic acid. This confirms the findings of the previous studies that an increase in the length of saturated acids reduces their stabilization efficiency in respect to magnetic fluids. The study has been carried out in collaboration with the Department of Physics, Taras Shevchenko National University of Kyiv (Kiev, Ukraine) and the Wigner Research Centre of the Hungarian Academy of Sciences (Budapest, Hungary).

1.3. Investigations of carbon nanomaterials

The biophysical research of fullerene solutions, in particular aqueous solutions of C60 and C70, has been continued. They included the analysis of the cluster structure when placing fullerenes in physiological environment and the study of the interaction of C60 fullerene with antitumor antibiotics, **Fig. 1-I-8** [12, 13]. Using SANS and tests on mutagenic activity of Doxorubicin and C60 admixture with Doxorubicin on Salmonella Typhimurium TA98 cells it has been shown that fullerene C60 can act as an interceptor of the antitumor antibiotic Doxorubicin and form hetero-complexes with this drug.

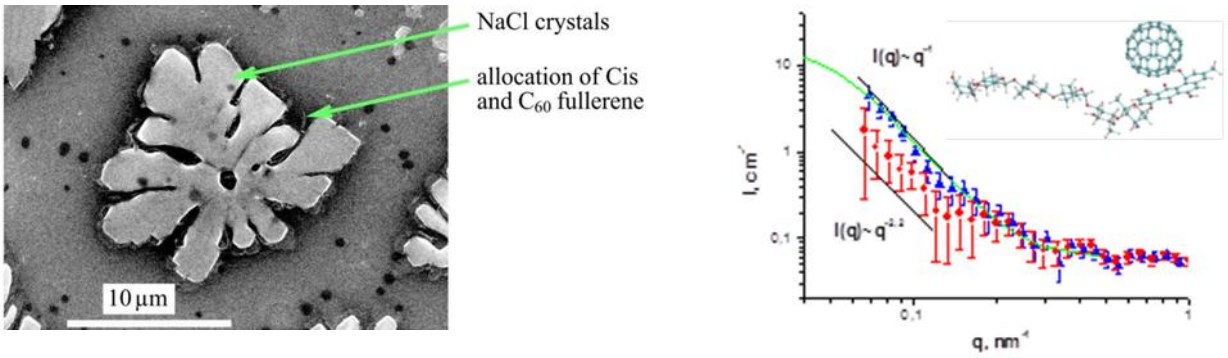

(a) (b)

***Fig. 1-I-8**. SEM data for C60/Cisplatin solution (a). SANS for aqueous C60 solution (blue triangles) and mixture of C60 with Landomycin A (red circles). The green line corresponds to the model curve obtained from the inverse Fourier transform. Insert: estimated structure of C60 + Landomycin A complex (b).*

The research on the interaction of C60 with Doxorubicin, including SANS, scanning electron (SEM) and atomic force (AFM) microscopy, calorimetry, dynamic light scattering (DLS) and UV-Vis spectroscopy, has been extended to include other aromatic drugs with a similar to Doxorubicin spatial structure such as Landomycin and Cisplatin. New effects of the biological interaction of fullerene C60 in combination with various anticancer drugs have been discovered and described. The work was carried out in collaboration with the Departments of Biology and Physics, Taras Shevchenko National University of Kyiv (Kiev, Ukraine).

The investigations related to the structural characterization of aqueous dispersions of detonation nanodiamonds (DND) have been continued [14]. In particular, the structures of DND hydrogels with a positive ζ-potential have been studied. The results of the SANS contrast variation have been compared with the data of the previous similar experiments for DND suspensions with a negative ζ-potential. No principal differences from a structural viewpoint between ζ+ and ζ- stabilizations of aqueous DND suspensions have been found. The identity of the structure on the size scale up to 100 nm has been proved with respect to the developed clusters characterized by similar values of fractal dimensions, as well as to the DND particles characterized by polydispersity (above 30%) and diffuse surface. This demonstrates the existence of a common mechanism for

DND cluster formation and growth in suspensions, regardless of the method of stabilization. It has been assumed that nanosystems are stabilized by the formation of a charged interface around the whole clusters rather than around individual particles in them. The study has been carried out in collaboration with the Ioffe Physical-Technical Institute RAS (Saint-Petersburg, Russia) and the Department of Physics, Taras Shevchenko National University of Kyiv (Kiev, Ukraine).

1.4. Investigation of layered nanostructures

In the framework of the studies on improving the performance of lithium batteries, a series of experiments on neutron reflectometry (GRAINS reflectometer) to study electrochemical interfaces of liquid electrolyte/solid electrode have been carried out (**Fig. 1-I-9**). From the specular reflectivity analysis, the formation of a solid-electrolyte interphase (SEI) on the surface of the electrode (Cu) has been concluded, as well as the lithium electrodeposition and growth of parasitic dendritic structures during the operation of an electrochemical cell have been tracked.

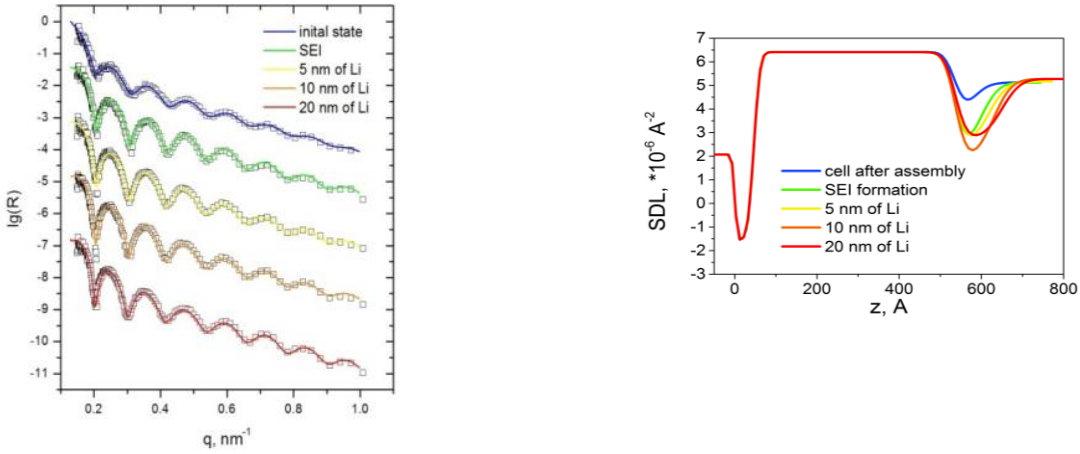

(a) (b)

Fig. 1-I-9*. (a) Experimental neutron specular reflectivity curves (points) for a copper electrode at the interface with the electrolyte at different current and voltage supply modes. (b) Resulting scattering length density profiles for different modes presented in (a) with indicated characteristic thicknesses of deposited lithium.*

The obtained profiles of the scattering length density perpendicular to the electrode surface have made it possible to analyze different modes of SEI formation, as well as the formation and growth of nanometer lithium layers of different roughness on the initially formed SEI. It has been shown that neutron reflectometry can be effectively used for *in situ* characterization of lithium plating on metal electrodes [15]. The study has been performed in collaboration with the Department of Chemistry, Moscow State University (Moscow, Russia).

In layered structures S1/FM/S2 consisting of ferromagnetic and superconducting layers, the effect of superconductivity on ferromagnetism has been studied by using reflectivity and scattering of polarized neutrons. It has been shown experimentally that at low temperatures magnetic structures with linear dimensions in the range from 5 nm to 30 μm are formed. At temperatures below the superconducting transition, the magnetization of the magnetic structures in the vanadium and niobium layers is suppressed by superconductivity. **Figure 1-I-10** demonstrates for different structures that the neutron scattering diminishes as the temperature decreases from 8 to 1.5 K.

Also, **Fig. 1-I-10** shows how the structure of the cluster system at 8K is transformed into the structure at 1.5 K.

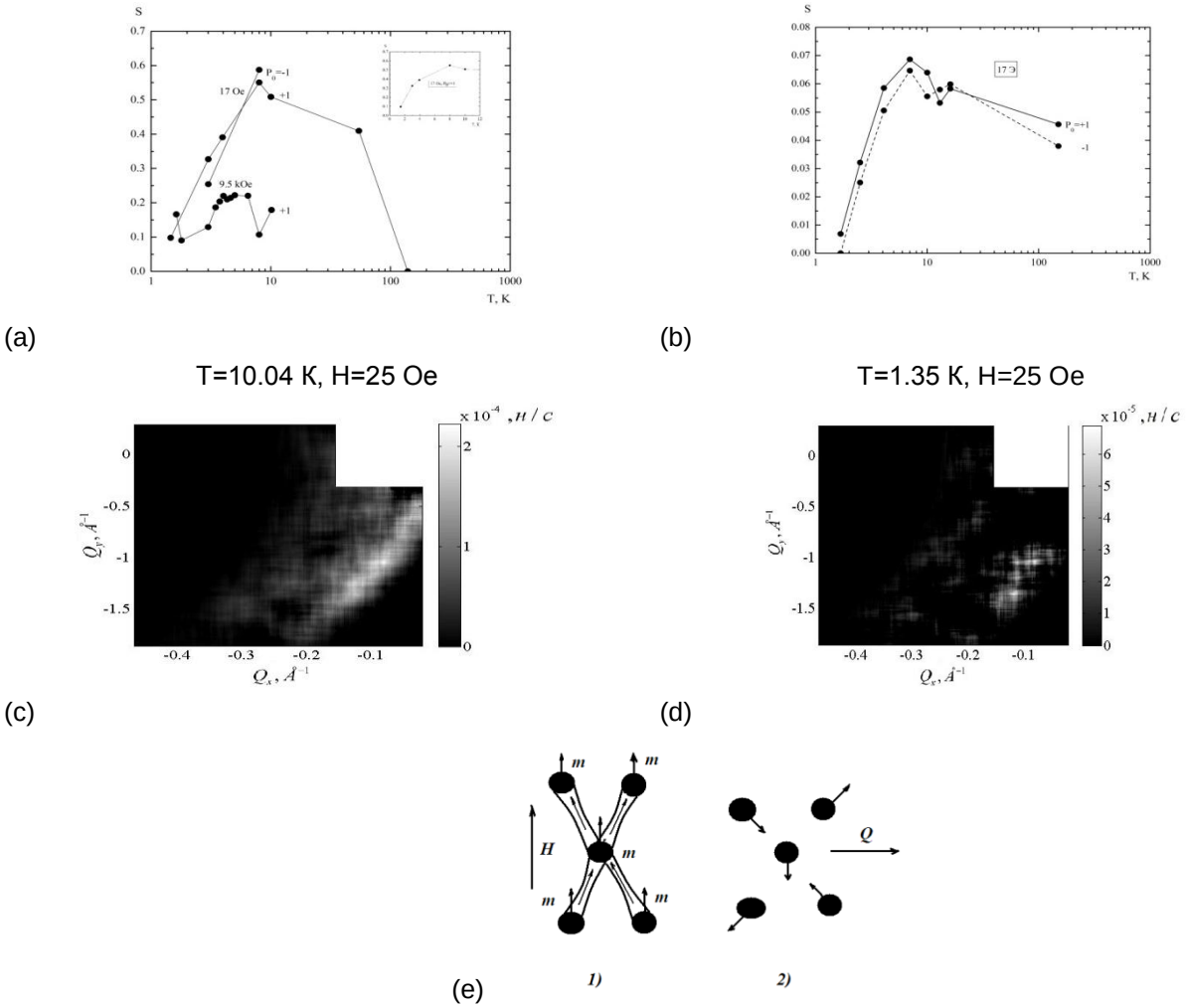

***Fig. 1-I-10**. Dependence of the neutron scattering coefficient S(T) for the structure V(150nm)/(FM(7%)+V(50%)+Nb(43%)(25 nm))/Nb(150 nm) at H = 17 Oe and 9.5 kOe (a). The dependence of the neutron scattering coefficient S(T) for the structure V(150nm)/(FM(7%)+V(43%)+Nb(43%)+Cr(7%))(25 nm)/Nb(150 nm) at H = 17 Oe (b). The contours of the neutron scattering intensity on the plane of transfer wave vectors Qy-Qx at H = 25 Oe and T = 10.04 K (c) and 1.35 K (d). The structure of the cluster system at 8 K (1) and 1.5 K (2) (e).*

Using the *in situ* reflectometry of polarized neutrons the magnetic state of a superconducting-ferromagnetic layered structure Ta/V/FM/Nb/Si has been studied. The relaxation of a non-uniform magnetic state of the structure with a characteristic time of a few hours was observed at temperatures both above and below the superconducting transition points in the structure layers. The character of the time dependence of the neutron scattering depends on the magnitude of the magnetic field H, temperature and neutron polarization. **Figure 1-I-11** shows the time dependence for the coefficient of neutron scattering. The dependence on polarization due to the scattering from magnetic clusters can be seen. The moments of the clusters are reoriented from the initial direction along the field to the direction against the field. There is also a scattering contribution which is independent of polarization and caused by the formation of a domain structure with time.

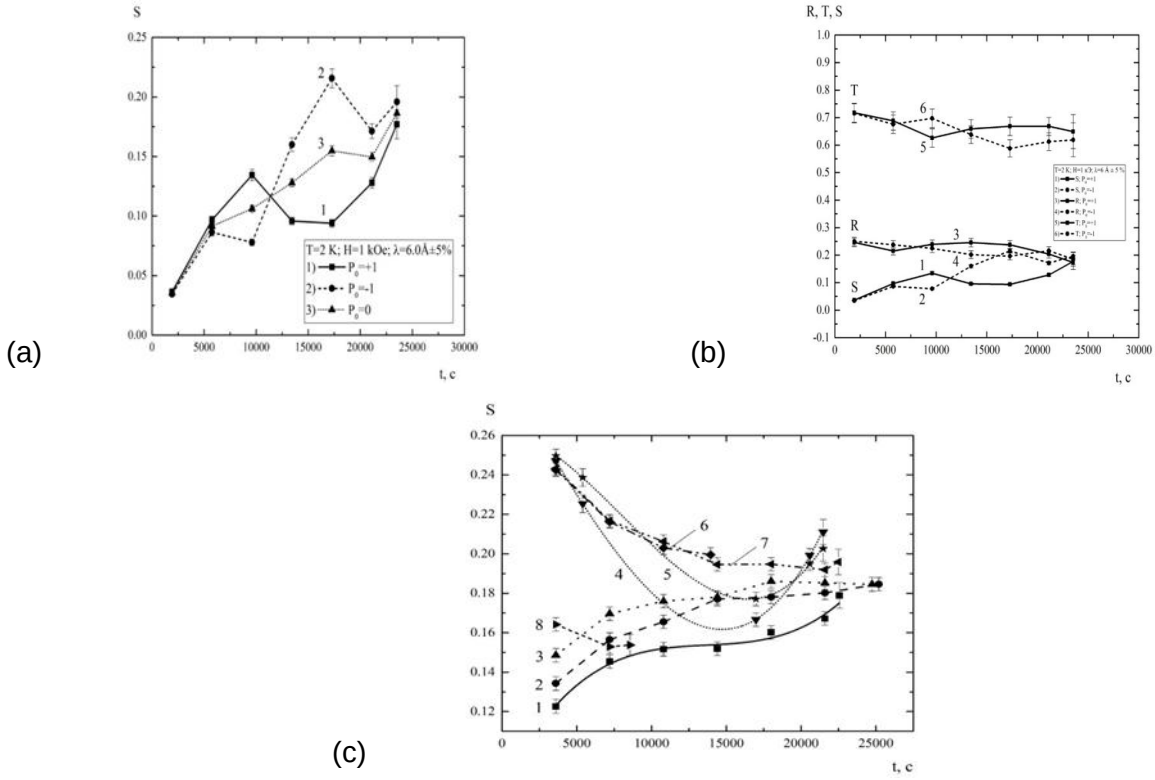

***Fig. 1-I-11**. Dependence S(t) in magnetic field of 1 kOe at temperature of 2 K for λ = 6 Å and P_0 = +1, –1 and 0 (a). Time dependences for coefficients of transmission T, reflection R and scattering S (b). Dependence S(t) at T = 3 K: P_0 = +1 at H-values: 17 Oe (1), 1 kOe (2), 2 kOe (3), 4 kOe (4), 6 kOe (6), 7 kOe (7) and 8 kOe (8); P_0 = –1 and H = 4 kOe (5) (c).*

At a large field of 4 kOe (curves 4 and 5, **Fig. 1-I-11(c)**), in early stages there is a depinning of superconducting vortices in the mixed state of superconducting layers of vanadium and niobium, which is changed to the motion of cluster moments.

Thus, apparently it was for the first time when neutron reflectometry (coherent propagation - reflection and transmission, as well as GISANS) was used to study the relaxation of the magnetic state and observe relaxation in a hybrid structure consisting of ferromagnetic and superconducting layers. In this case, the characteristic time of the change in the magnetic state of the systems of clusters, domains and vortices was a few hours with a several percent accuracy in the time dependence measurement. The measurement of the time dependences for the coefficients of scattering, reflection and transmission occurring under changes in the average and local potentials of the interaction of neutrons with the medium, was an effective method for identifying types of magnetic systems in the layered structures. In principle, a potential increase in the intensity of the neutron beam at the REMUR spectrometer used in the present study could allow one to achieve time resolution of a few minutes in studies of irreversible processes.

1.5. Investigation of biological nanosystems, lipid membranes and lipid complexes

It is well known that fermentative systems of oxidative phosphorylation in mitochondria can operate in two states - in a state of supercomplex and in a dissociated state. The comprehensive studies have shown that heart mitochondria operate in the state of supercomplex in a wide range of tonicities of incubation media. This result has been obtained by the polarographic method using

the double inhibitor technique by Baum. The investigation of mitochondrial ultrastructure by the methods of electron microscopy (EM) and small-angle neutron scattering (SANS) under conditions of normal tonicity (300 mOsm - isotonia) and low-amplitude swelling (120 mOsm - hypotonia) has proved the existence of two types of mitochondrial ultrastructure. Using EM, it has been found that the mitochondrial cristae in hypotonic and isotonic conditions have different shape and thickness. The tomography method has demonstrated a folded configuration of the cristae. The studies of the ultrastructure of heart mitochondria by methods of EM and inhibition analysis have been carried out on intact functioning mitochondria in the presence of respiratory substrates. Using the SANS method it has been shown that in hypotonic and isotonic media highly-organized lipid-protein lamellar structures are formed in mitochondria. The formation of lipid structures has been demonstrated by using the contrast variation technique (variation of the fraction of heavy water in a solution). Also, it has been shown that the thickness of the mitochondrial cristae depends on the medium tonicity. Thus, the data obtained from the investigation of the functioning and structure of mitochondria suggest the existence of two states for the system of oxidative phosphorylation, which forms cristae with different structural parameters [16].

The passive transport of particles through lipid membranes in different lipid phase states has been investigated by inelastic X-ray scattering. It is known that the passive transport of molecules through a cell membrane depends on thermal motions of lipids. However, the nature of transmembrane transport and its precise mechanism are not fully understood. The phonon excitations in a lipid bilayer of 1,2-dipalmitoyl-*sn*-glycero-3-phosphocholine above and below the main phase transition temperature have been measured. In the gel phase, for the first time the presence of transverse high-frequency modes has been shown. The modes are terminated when the lipids change into the liquid phase. This termination is apparently due to the formation of short-lived nanometer lipid clusters and transient pores which facilitate the passive molecular transport through the lipid bilayer. The obtained data suggest that the phononic motion of the lipid hydrocarbon tails provides an effective mechanism of passive transport [17].

The investigations (diffraction and small-angle scattering of neutrons and synchrotron radiation) of lipid membranes and nanoparticles on their basis have been continued in collaboration with the University of Messina, Italy, and NRC "Kurchatov Institute". The structural organization of vesicular drug carriers, including a vesicular transport system Phospholipovit, has been studied (**Fig. 1-I-12**) [18].

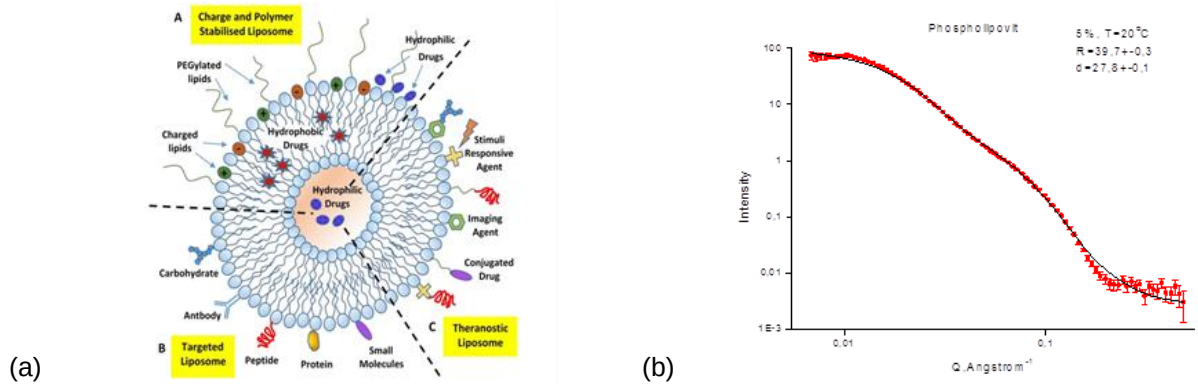

***Fig. 1-I-12**. Schematic representation of vesicular transport systems of various types for drug delivery (a). Experimental and calculated curves of small-angle neutron scattering (YuMO) for vesicular transport system Phospholipovit (b).*

Particular attention has been given to the processes of interaction and aggregation of vesicles. The general principles of the organization of vesicular drug carriers have been formulated.

1. SCIENTIFIC RESEARCH

In the framework of the study of the structure and properties of membranes the experiments on molecular dynamics simulation (MD) and SANS for Ca2+ and Zn2+ cations with the gel phase of a model lipid membrane of dipalmitoylphosphatidylcholine (DPPC) have been carried out. As a result, the formation of oriented multilamellar membranes has been studied. An increase in the bilayer thickness has been revealed for both considered cations at a molar ratio of divalent metal ion to lipid (Me2+:DPPC) of ~1:7. The MD simulations have made it possible to reveal a slight difference in the effect of the cations on the gel-phase of membranes. The study [19] has been performed in collaboration with the Comenius University (Bratislava, Slovakia), a number of research laboratories in the USA and LRB JINR.

Comprehensive studies of the phase transitions, morphology and internal structure of an organogel of 4-heptyloxyphenylolithocholic acid (7OPhOLCA) – a derivative of lithocholic acid (LCA) have been carried out. The obtaining of stable organogels with specified chemical and physical properties is a challenging direction regarding the potential applications in optoelectronics, drug delivery in medicine, regeneration of damaged tissues, etc. The samples of 7OPhOLCA in DMSO-d6 with various concentrations have been studied by the SANS method, as well as temperature ranges for the sol-gel transition have been determined, **Fig. 1-I-13** [20].

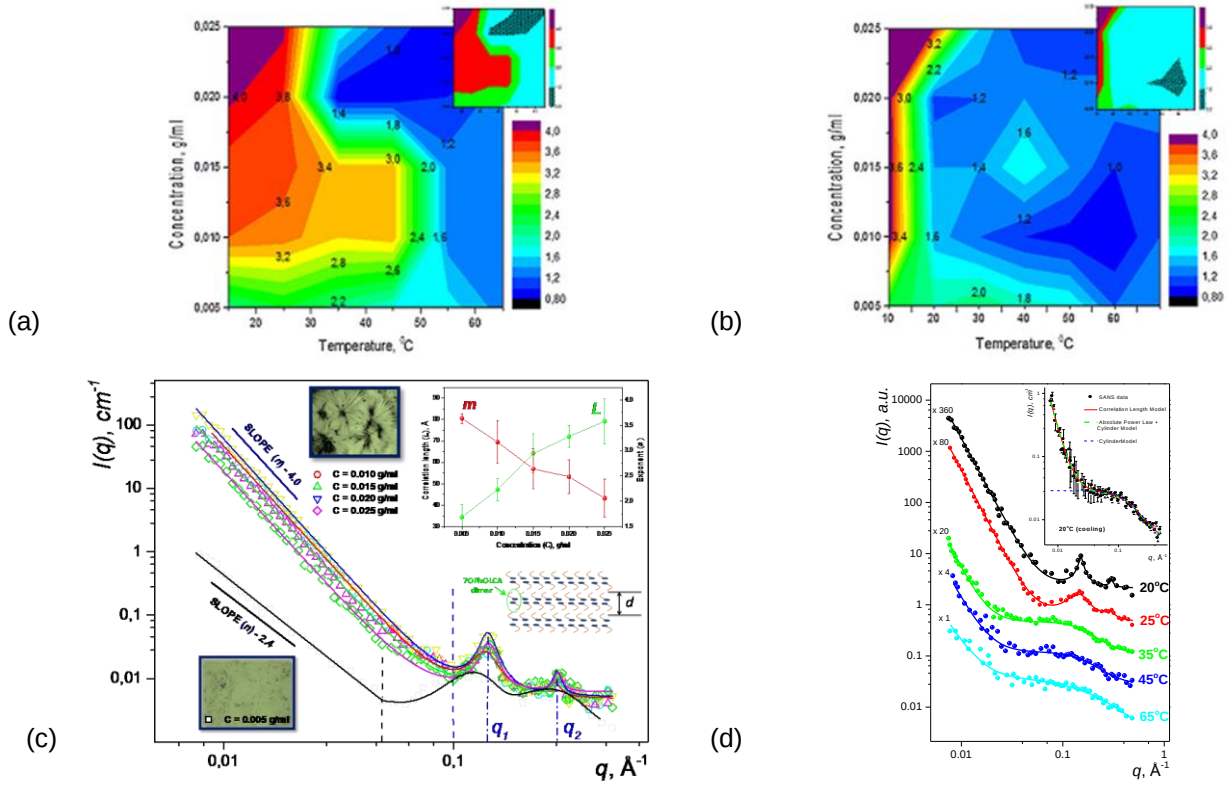

Fig. 1-I-13*. Sol-gel transition for heating (a) and cooling (b). SANS curves (symbols) with fits (lines) for 7OPhOLCA in DMSO-d6 at concentration C = 0,005, 0,010, 0,015, 0,020, and 0.025 g/ml at T = 10 ℃ after a single heating-cooling cycle (c). Dashed vertical lines divide the ranges of small and large q-values; q_1 and q_2 correspond to the maximum intensity of Bragg peaks. Optical microscopy images were obtained for samples stabilized for 12 hours in quartz cells at T = 10 ℃. Insert: change in the correlation length, L, and the exponent, m, as a function of concentration of 7OPhOLCA. Changes in the SANS curves with increasing temperature for 7OPhOLCA in DMSO-d6 at C = 0.015g/ml (d). Insert: SANS curves (circles) at T = 20 ℃ during cooling.*

It has been shown that the transition temperature decreases with increasing concentration of organogel when heated. The reason for the changes in the internal structure around the sol-gel transition is the destruction of hydrogen bonds, as shown by IR spectroscopy. Furthermore, the analysis of small-angle scattering curves has revealed morphological changes of the studied samples in the gel phase, which had not been initially detected by DSC because of low enthalpy (compared to the phase transitions). In particular, at temperatures above 25°C the lamellar organization of dimers is destroyed.
At the same time, no reorganization of hydroxyl groups is observed (IR spectroscopy). In the analysis of the SANS data three models have been proposed. The time stability of organogels has also been studied. It has been found that all the phases observed are reversible and the structure of the studied samples exhibits a memory effect.

1.6. Polymeric materials

Small-angle neutron scattering has been used to study the structural peculiarities of perfluorinated proton conducting polymer samples containing sulfonic groups of Aquivion. A fine structure of polymeric membranes based on a system of proton conducting channels in a perfluorinated polymer matrix has been revealed. The way this fine structure changes has been determined as a function of the equivalent weight of the membrane, and the relation of these changes with the proton conductivity value has also been established. The contrast variation technique has made it possible to study the effect of orientational stretching on the fine structure. It has been found that the stretching is accompanied by an increase in the proton conductivity due to changes in the fine structure of the channel system. Our investigations confirm that a reduction of the side chain length affects the fine structure of the perfluorinated proton conducting membranes. This is accompanied by an improvement in their performance in hydrogen fuel cells [21].

Silver sols synthesized in polymer matrices have been investigated by small-angle X-ray scattering (SAXS) in combination with ultraviolet-visible (UV-VIS) spectroscopy and quasielastic light scattering (QELS). The characteristics of the particle size distribution obtained by each of the methods are in good agreement. It has also been found that there are deviations of the experimentally measured characteristics from the existing theoretical models. The most likely reason for this is that the nanoparticle clusters have a non-spherical shape [22].

The modeling of the glass transition kinetics for polystyrene has been continued. Using different theoretical methods currently applied to polymer systems, a single measurement of the temperature dependence for the heat capacity under heating and cooling has been modeled. It has been shown that for single curves good agreement is achieved, however the resulting model parameters do not allow one to describe correctly the dependence of the glass transition temperature on the cooling rate. In the opposite case, if the dependence $T_g(q)$ is fitted the agreement with a single measurement is of poor quality. Thus, it has been clearly shown that the modeling of glass transition in terms of the general parameters depending on the cooling rate simultaneously with the transition kinetics is impossible within the framework of the existing models [23]. The study has been performed in collaboration with the University of Rostock (Rostock, Germany).

1.7. Atomic and molecular dynamics

Inhibitors of 3-hydroxy-3-methylglutaryl coenzyme A (HMG-CoA) reductase are among the most effective and widely used drugs for lowering the cholesterol level, known as statins. Statin monotherapy is generally well tolerated and has minimal side effects. The first HMG-CoA inhibitor approved by FDA (Food and Drug Administration, USA) – lovastatin (MEVACOR®; ALTOCOR® &

1. SCIENTIFIC RESEARCH

ALTOPREV®), below referred to as LOV was mainly used to control hypercholesterolemia (**Fig. 1-I-14**).

In the LOV molecule three main parts can be distinguished – lactone ring (lct), naphthalene fragment (nph) and methylbutanoate chain (mbt). The molecules are linked by hydrogen bonds O···HO (**Fig. 1-I-14**). Hydrogen bonds bind lactone rings (methyl group) with methylbutanoate chains (carbonyl group). The second carbonyl group of lactone rings is unbound.

(a)

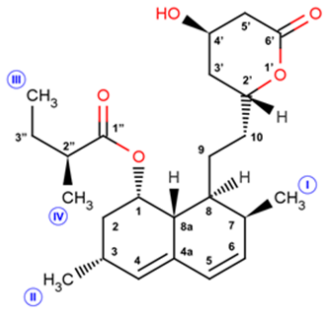

(b)

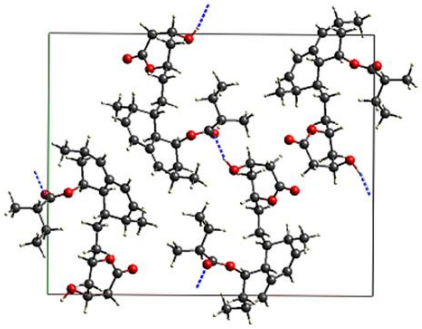

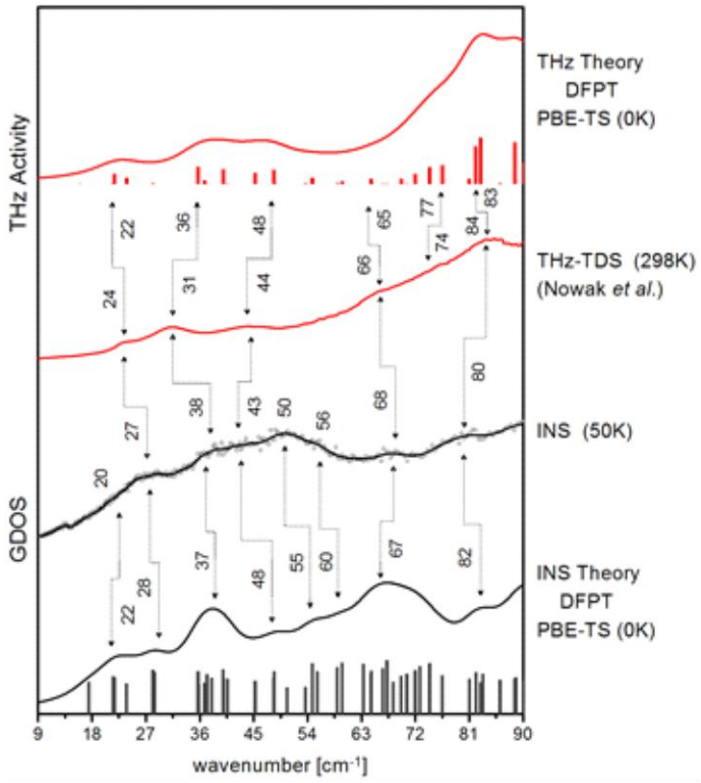

(c)

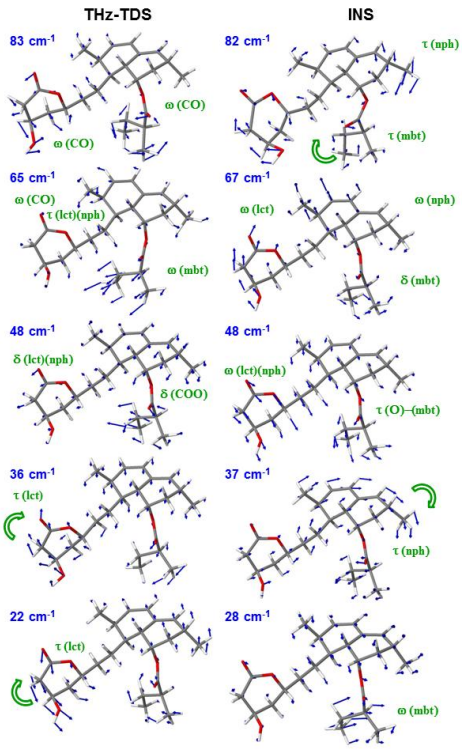

(d)

***Fig.1-I-14**. Molecular formula of lovastatin (LOV; (1S,3R,7S,8S,8aR)-8-{2-[(2R,4R)-4-Hydroxy-6-oxooxan-2-yl]ethyl}-3,7-dimethyl-1,2,3,7,8,8a-hexahydronaphthalen-1-yl (2S)-2-methylbutanoate) with marked methyl groups (I-IV) (a). Crystal structure of lovastatin (space group $P2_12_12_1$) optimized using PW - DFT (PBE-TS) (b). Comparison of theoretically calculated (harmonic approximation DFPT PBE-TS) and experimental vibrational spectra of lovastatin according to the data of neutron (IINS) and optical terahertz spectroscopy (data by Nowak et al. Acta Poloniae Pharmaceutica in Drug Research, Vol. 72 No. 5 (2015) pp. 851-866) (c). The most important vibrational modes of lovastatin contributing to the INS and THz-TDS spectra. The eigenvectors obtained from the harmonic PBE-TS calculations are shown in the projection of one molecule(d).*

In collaboration with the Adam Mickiewicz University (Poznan, Poland), atomic and molecular dynamics of lovastatin has been studied by ^{1}H NMR and inelastic neutron scattering complemented by theoretical ab-initio calculations using the PW-DFT method. A consistent molecular dynamics model has been obtained, which can be later used to describe the dynamics of other alternative drug forms and tendencies to amorphization. It has been found that the molecular dynamics of lovastatin is determined by the motions of methyl groups and the conformational disorder in the methylbutanoate fragment. The vibrational dynamics of lovastatin was analyzed focusing on the energy transfer range with low wave numbers, which was experimentally studied by neutron (INS) and terahertz (THz-TDS) spectroscopy. The theoretical calculations made it possible for the first time to describe with a high accuracy the phonon spectrum of lovastatin in this region (**Fig. 1-I-14**).

It should be noted that the main contribution to the inelastic neutron scattering spectra is from vibrations of hydrogen-containing molecular groups, which are the most mobile ones for the movable mbt fragment contributing to the most intense vibrational mode. At the same time, the primary contribution to the terahertz spectra is from the most polar molecular groups containing oxygen and included in the lct fragment. The corresponding normal vibrational modes are shown in **Fig. 1-I-14**. The most intensive spectral features for THz-TDS are due to the modes related to the vibrations of hydrogen bridges O···O in a range of above 65 cm^{-1}, while the modes in a range of below 65 cm^{-1} are determined by the vibrations of the whole lct fragment. This set of modes is of a general nature without intending to be bound to a particular LOV compound and can be used in further studies of statins.

The experimental and theoretical investigations of the dynamics of a nitrated derivative of ortho-hydroxy acetophenone have been carried out. To estimate the barriers of the conformational changes and folding, the potential barriers for the nitro group rotation and hydroxyl group isomerization were calculated. Two polymorphic forms of this compound were obtained by slow and rapid evaporation of the polar and nonpolar solutions, respectively. Both polymorphs were investigated by means of infrared, Raman and neutron spectroscopy (**Fig. I-15**), nuclear quadrupole resonance, differential scanning calorimetry, and theoretical calculations using the DFT method were performed as well. In one of the polymorphs phase transitions were detected.

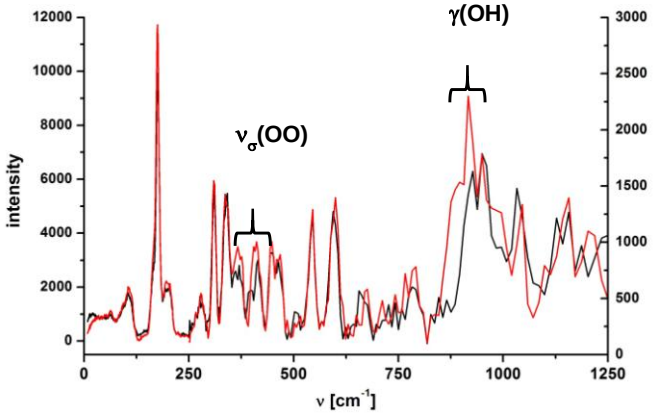

***Fig. 1-I-15**. Spectra of inelastic scattering (NERA, IBR-2, JINR) from polymorphic forms of o-hydroxy-acetophenone (red line) and its mono-deuterated analogue. The left and right Y-scales correspond to the spectral ranges of 0-250 cm^{-1} and 250-1250 cm^{-1}.*

The position of the nitro group and its influence on the crystal structure were analyzed by X-ray diffraction. A full spectrum analysis of the vibrational spectra for the interpretation of the two

conformations was performed. On the basis of the obtained data the nature of the phase transition has been explained [24].

1.8. Applied research

On FSD, the experiments to study the distribution of residual stresses in welds after using various welding methods have been continued. The work has been carried out in collaboration with the Institute of Electronics, BAS (Sofia, Bulgaria) and the Brandenburg University of Technology (Germany). In 2016, residual stresses were measured in a massive (thickness ~ 20 mm) sample from structural steel S355J2+N welded with combined multipass welding: 1st pass – metal welding in shielding gases (MSG-welding), 2nd and 3rd passes – submerged arc welding (SAW-welding), **Fig. 1-I-16**.

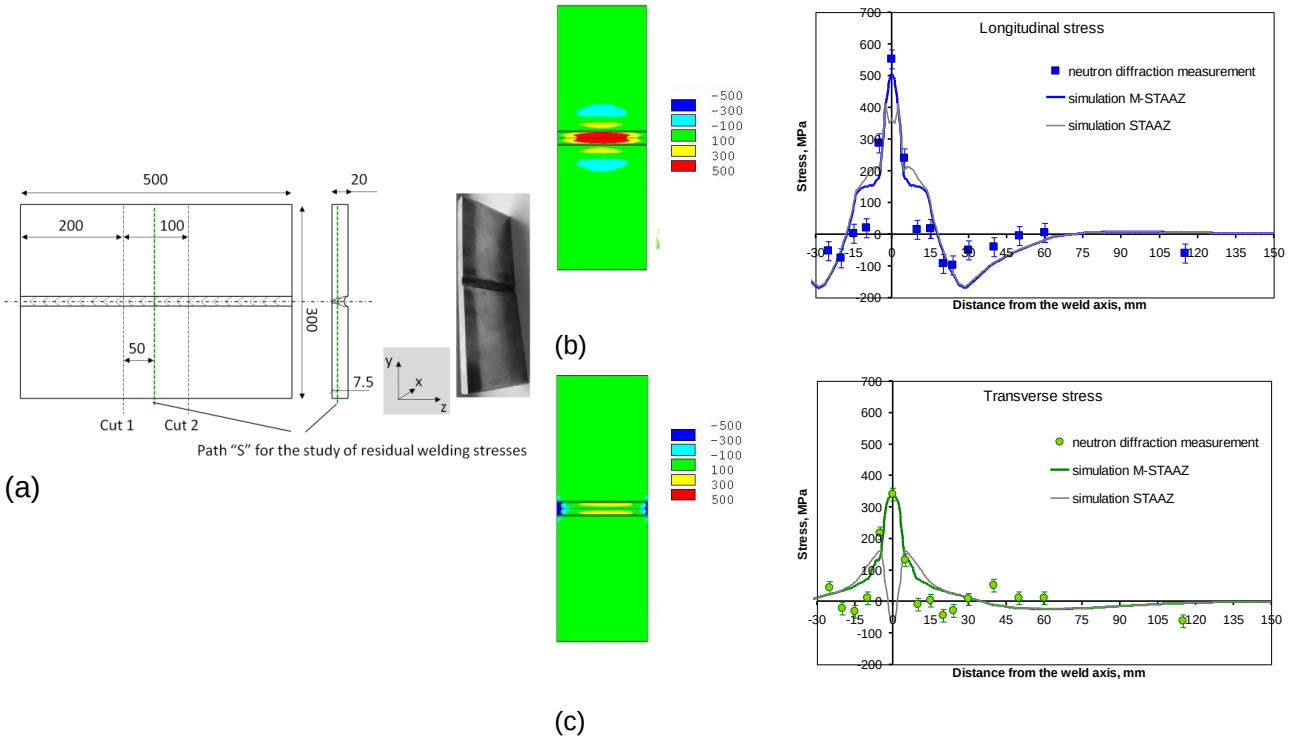

***Fig.1-I-16**. Sample cut from a thick (~ 20 mm) plate welded with multi-pass submerged arc welding (SAW-welding). "S" is a scan-line in neutron measurements. Arrows indicate the strain tensor components (X, Y, Z) (a). Full map of distribution of the longitudinal component (σ_X) in the tensor of residual stresses calculated by the finite element method (FEM) and the comparison of the experimentally measured σ_X-values along the scan-line "S" with the results of numerical modeling by FEM (solid line) (b) . Full map of distribution of the transverse component (σ_Y) in the tensor of residual stresses calculated by FEM and the comparison of the experimentally measured σ_Y-values along the scan-line "S" with the results of the numerical modeling by FEM (solid line) (c).*

In neutron experiments with new radial collimators in the middle part of the sample the residual stress tensor components were measured in a wide X-range across the weld, which were further used to determine the residual stress values (**Fig. 1-I-16**). The maximum component is the longitudinal stress tensor component σ_x (~ 550 MPa) directed along the weld which is of the stretching character in the center of the weld. The level of the transverse component of the stress

tensor σ_y is significantly lower (~350 MPa), and the level of the normal component σ_z does not exceed 180 MPa.

In addition to the experiments on neutron diffraction, numerical calculations by the STAAZ method have been performed in the framework of the existing cooperation with the research group of Prof. V. Mikhailov (Brandenburg University of Technology, Germany). The comparison of the neutron data and FEM calculations has shown good agreement, indicating the reliability of the developed theoretical model for the multi-pass welding process. This information can serve as a basis for the development of specific technical recommendations to achieve the desired level and profile of residual stresses.

On FSD, a series of TRIP-composites with austenitic matrix and different content of reinforcing ceramic phase of zirconium dioxide ZrO_2 partially stabilized by magnesium (Mg-PSZ) have been investigated at various degrees of plastic deformation (uniaxial compressive load), **Fig. 1-I-17**.

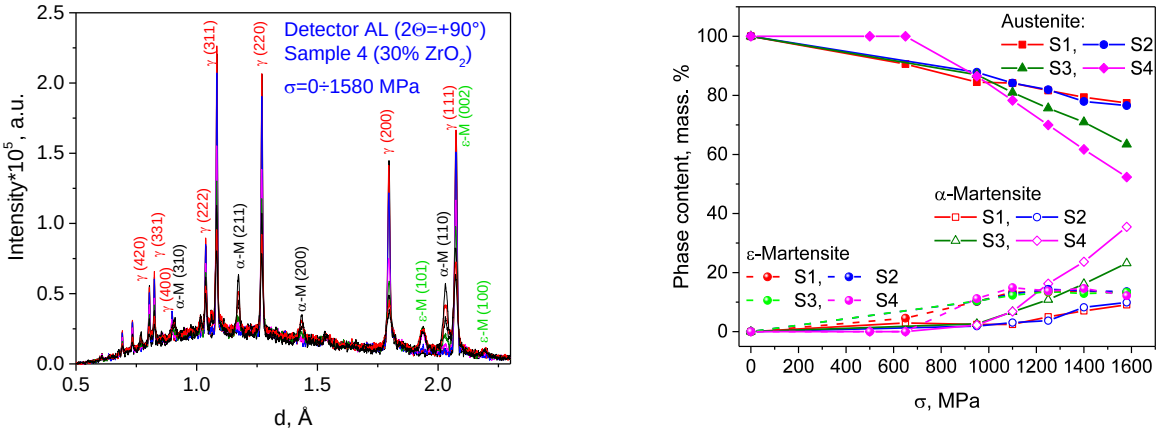

(a) (b)

***Fig. 1-I-17**. The change in the diffraction spectra of the TRIP-composites as a function of plastic deformation (a). The change in the phase mass content in the TRIP composites depending on the degree of plastic deformation (b).*

The study has been done in collaboration with the Freiberg University of Mining and Technology (Freiberg, Germany). At the load values above 650 MPa, the formation of two phases in the austenitic matrix was observed: cubic α'-martensite and hexagonal ε-martensite. The content of ε-martensite reached ~15% for all samples under deformation up to σ = 1100 MPa and then remained almost unchanged until the maximum load values of σ = 1580 MPa. In contrast, the α'-martensite phase exhibited a monotonic increase in the load range from 950 to 1580 MPa. In the ceramic sample of pure zirconium dioxide (100% ZrO_2) two phases were observed: cubic (f ≈ 55%) and tetragonal (f ≈ 45%). The residual deformation of the crystal lattice of the austenitic matrix is of compressive character and increases up to ~10^{-3}. In this case, the crystal lattice deformation in α'- and ε-martensites is more complex and reflects the redistribution of the load between the phases. Furthermore, under the deformation in the range from 650 to 1580 MPa a noticeable broadening of the diffraction peaks with increasing plastic deformation was observed, which was caused by the variation in the contrast factor of dislocations. For the austenitic matrix the dislocation densities were evaluated from the peak broadening. They reached the values in the range of $12÷20\cdot10^{14}$ m^{-2} depending on the content of zirconium dioxide in the composite.

1. SCIENTIFIC RESEARCH

The texture and microstructure of the pristine and retrogressed samples of eclogite and surrounding metasediments have been investigated to gain insights into the deformation processes in the palaeo-subduction channel of the Tauern region (Austria), **Fig. 1-I-18** [25]. The texture features and deformation processes in omphacite and glaucophane have been analyzed. The presence of a plastic deformation cycle in the metamorphism of eclogite and blueschist facies associated with the subduction and exhumation of rocks has been established.

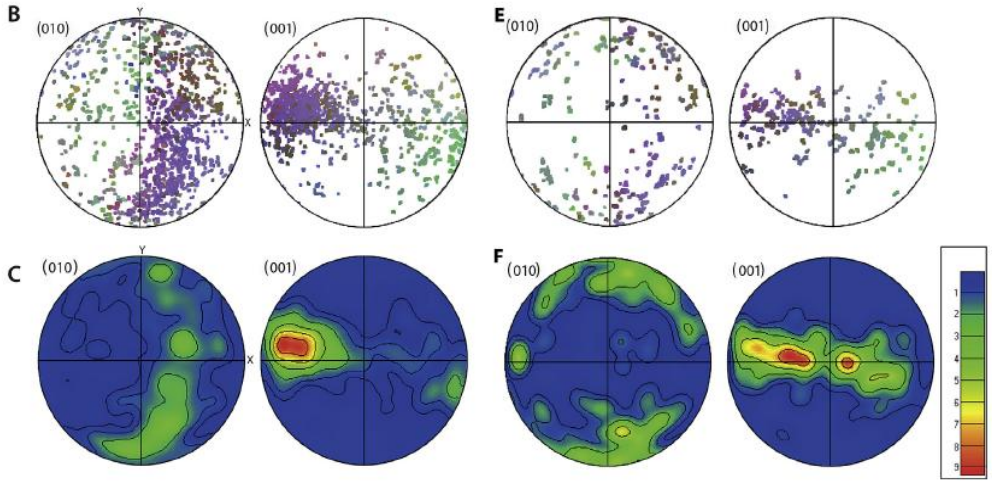

***Fig. 1-I-18**. Pole figures for eclogite rocks obtained with the SKAT diffractometer.*

A new approach has been developed for a quantitative comparison of pole figures with the same crystallographic indexes, but measured for different samples. The approach is based on the consideration of the measured pole figures as specific implementations of a certain orientation distribution, i.e., as samples from a general ensemble of orientations. Thus, for the first time in the texture analysis a statistically valid measure for the quantitative comparison of pole figures has been introduced. This measure is the probability that the samples belong to the same orientation distribution and follows the statistics calculated within the Kolmogorov-Smirnov statistical test. The application of the introduced measure has been demonstrated on numerical examples for materials with cubic and hexagonal symmetry, as well as for real experimental data (pole figures of wheel steel). Also, using numerical examples, the peculiarities of the new approach have been demonstrated in comparison with the traditional calculation of the RP value when comparing pole figures [26].

The work has been done on the development of the methodology for evaluating the amount of residual austenite in high strength steels using the neutron diffraction method. The neutron diffraction spectra were measured on the texture instrument SKAT at FLNP JINR in order to eliminate the influence of the texture on the results. The measurements of calibration samples with the known austenite content were made. Using the results from the measurements of these samples, the calibration lines were obtained and applied to determine the fraction of residual austenite in the samples of medium-carbon steels (0.3 to 0.4%) with a tensile strength of 1500 MPa and 1700 MPa at different annealing temperatures (150 to 400ºC) following the hardening treatment [27].

On the EPSILON diffractometer, *in-situ* experiments to study the dependence of deformation on the load on a cylindrical sample of sandstone have been carried out (**Fig. 1-I-19**). A load of up to 56.33 MPa was applied during 9 stages to determine the Young's modulus for the crystallographic planes of quartz (01-11), (10-11), (11-20), (01-12)/(10-12). These results are

consistent with the Hooke's law [28]. Instead of traditional fitting of diffraction data using the Rietveld method, an elastomechanical model has been developed to describe the stress-strain behavior, taking into account the changes in the pore space as a result of compaction of sediments associated with the change in the shape of quartz grains. This model was used to calculate the displacement of the diffraction peaks in the Voigt or Reuss approximations and their combinations. It has been established that the developed model can simulate with a high accuracy the diffraction data under load using the data measured without load including both the displacement of peaks and their half-width changes [29].

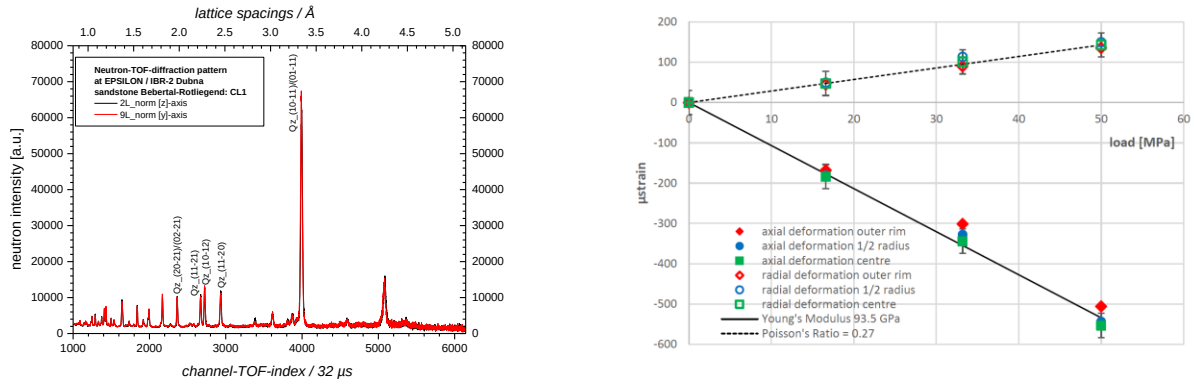

(a) (b)

***Fig. 1-I-19**. Neutron diffraction spectra of sandstone measured on the EPSILON diffractometer (a). Dependence of microstresses on the load at various deformation types (b).*

In collaboration with the Institute of archaeology, RAS, the internal organization of a series of objects of cultural heritage (antique coins, bracelets, crosses, etc.) has been studied at the facility of neutron radiography and tomography. As an example, **Fig. 1-I-20** illustrates the results of the study of an ancient bracelet, XIV century AD, from a recently discovered treasure in the city of Tver. A corrosion-coated part of the bracelet was investigated. Neutron tomography revealed the bracelet decor items made by gold-on-copper plating. The differences in the interaction of neutrons with gold and copper made it possible to reveal a decorative pattern on the bracelet hidden under corrosion.

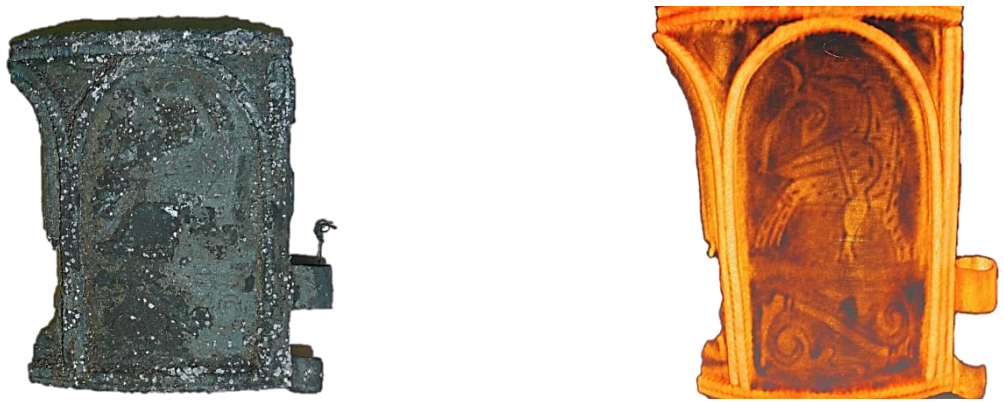

(a) (b)

***Fig. 1-I-20**. Photo of a fragment of the ancient bracelet from the treasure found in the city of Tver (a) and its 3D image reconstruction from neutron tomography data (b).*

2. Methodological results

A new mirror neutron guide (designed and manufactured by SwissNeutronics, Switzerland) has been installed on the HRFD diffractometer. New mirror sections have been mounted in the available vacuum housing with the entrance (behind Fourier chopper) and exit (in front of sample position) points remaining unchanged (total length of 18.8 m). The neutron guide has been designed to be plane-parallel in the horizontal plane (window width 15 mm) and have a parabolic convergence in the vertical plane (heights of the entrance and exit windows are 200 mm and 100 mm, respectively). The Ni/Ti supermirror glass coating has a critical index m = 1.75. The qualitative comparison of the effective scattering spectra from vanadium for the old and new neutron guides has shown that the overall spectrum shape has changed insignificantly, but a considerable shift towards shorter wavelengths by ≈0.6 Å has occurred (**Fig. 1-I-21**). The gain factor for the neutron flux was determined from the ratio of the intensities of the diffraction peaks from a standard sample of Al_2O_3 (**Fig. 1-I-21**). It can be seen that in the wavelength range from 2 to 7 Å its value varies from 2.2 to 2.7. At lower wavelengths, the new neutron guide gives even greater increase in the flux.

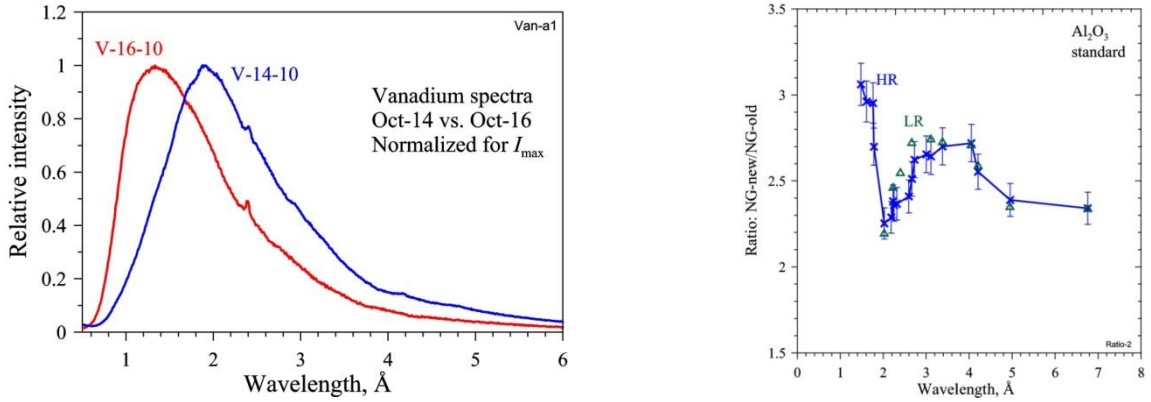

(a) (b)

***Fig. 1-I-21**. Qualitative comparison of effective spectra for old (V-14-10) and new (V-16-10) neutron guides using scattering from vanadium (a). Gain factor for the flux for the new neutron guide determined by comparing intensities of diffraction peaks from a standard Al_2O_3 sample as a function of wavelength (b). Points measured from spectra of high (HR) and low (LR) resolution, i.e. using correlation analysis and without it, respectively.*

On HRFD, the operation of a new Fourier chopper (**Fig. 1-I-22**) installed in August of 2016 to replace the old chopper has been started.

***Fig. 1-I-22**. New Fourier chopper in the working position.*

The Fourier chopper has been mounted on a movable platform to move/remove the chopper into/from the beam. This option is required in *in-situ* experiments performed on the HRFD diffractometer and provides an additional double increase in the flux for the high intensity mode.

A series of *in-situ* and *in-operando* neutron diffraction experiments using specially designed electrochemical cells have been carried out to determine optimal (from the viewpoint of neutron scattering) auxiliary materials for model current sources. Basic requirements to the materials are minimum incoherent scattering, minimum neutron absorption, ease of use in the assembly of the cell, in-store availability. An optimal separator, electrolyte and anode material have been selected (**Fig. 1-I-23**). The paper on the results of the work is under preparation. The demand for this work is testified by an increasing number of applications for experiments at the RTD and HRFD instruments with the use of the developed electrochemical cells.

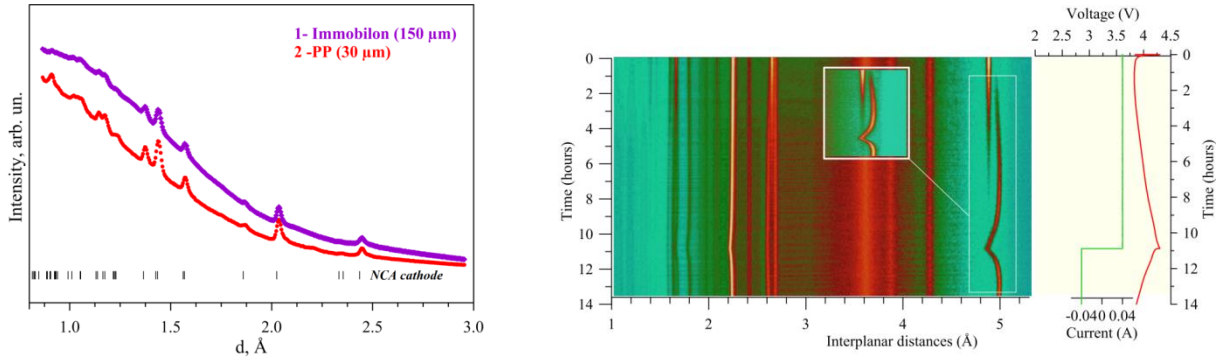

(a) (b)

***Fig. 1-I-23**. Comparison of neutron scattering from electrochemical cells with PVDF Immobilon and usual polypropylene separators (a). Immobilon (despite partial replacement of hydrogen with fluorine) is worse than normal separator because of a larger amount of absorbed electrolyte and resulting incoherent scattering. The evolution of the diffraction spectra obtained with the electrochemical cell with conventional electrolyte and separator during the first "forming" cycle (b). As a cathode, Li(Ni,Co,Al)O2 was used, as an anode – lithium-7 isotope. The marked region of diffraction peak 003 from the cathode clearly illustrates the cathode activation process over the entire electrode volume: intensity of gradually disappearing peak (top down) is directly proportional to the amount of inactive cathode material. After cell (battery) charging the entire volume of the cathode material is electrochemically active.*

In 2016, special cells for *in-operando* reflectometry experiments with electrochemical interfaces and a thermostatic cell with a temperature of up to 150°C were designed and successfully tested on the GRAINS instrument (**Fig. 1-I-24**).

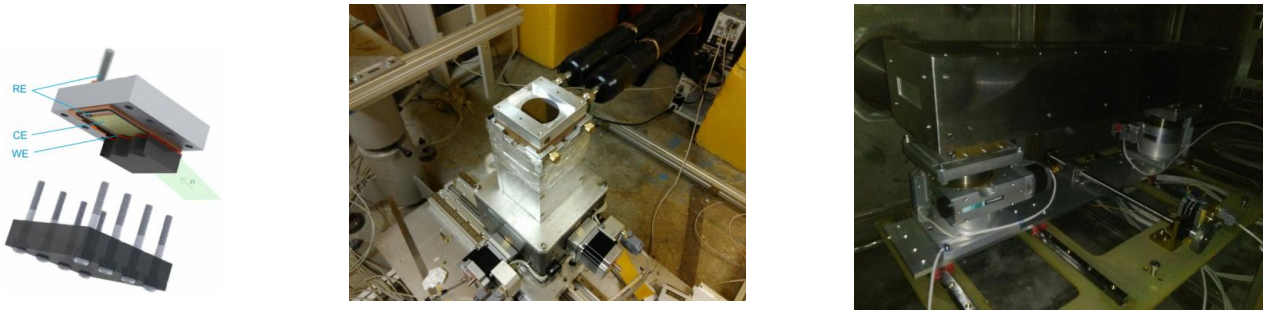

(a) (b) (c)

***Fig. 1-I-24**. Special three-electrode electrochemical cell (a) and thermostatic (up to 150 ℃) cell (b) for neutron reflectometry; automatic mobile platform with polarizer (c).*

1. SCIENTIFIC RESEARCH

An automatic mobile platform for the polarizer has been successfully put into operation at the GRAINS instrument for experiments with polarized neutrons.

Two new wide-aperture radial collimators (by JJ X-Ray, Denmark) have been installed at the FSD diffractometer, **Fig. 1-I-25**. To position the collimatiors, special tables that allow one to adjust the collimators in the scattered beam and to move/remove them into/from the beam if necessary, have been designed. The new radial collimators cover the entire angle range of ±20° in the scattering plane, thus allowing the use of all available elements of ASTRA detectors, which makes it possible to significantly increase the luminosity of experiments and perform measurements with thick samples.

(a) (b)

***Fig. 1-I-25**. New wide-aperture radial collimators for the FSD Fourier diffractometer, beamline 11A of the IBR-2 reactor (a). Bulk sample under study on the HUBER goniometer at FSD. Small scattering volume (gauge volume) within a sample is cut by the radial collimators mounted on special adjusting frames (b).*

On FSD, work to improve algorithms on obtaining diffraction spectra from "raw" data has been continued. In the list mode, a program has been developed to filter detection events and provide the same method of pulse duration discrimination as that implemented in the electronics of the ASTRA detectors at FSD. In addition, two new experimental operation modes of the Fourier chopper at FSD (Dirichlet and Blackman frequency windows) have been introduced, which will allow one to explore different dynamic aspects in the operation of the Fourier chopper and improve its control system.

On beamline 13 of IBR-2, the activities on the creation of the FSS Fourier diffractometer have been continued in collaboration with the SC department (**Fig. 1-I-26**). In 2016, the components of the Ost and West detectors were delivered to the beamline. Modules of a Huber goniometer were mounted and adapted to the table of FSS. A Fourier-chopper was installed on a platform and underwent idle testing. Crates with the detector and acquisition electronics were put in place. The state of the mirror coating in a section of the FSS neutron guide was studied with the GRAINS reflectometer, which revealed a significant damage of the mirror coating and the necessety to replace the sections of the neutron guide in the immediate future. The calculations of the new geometry for the Ost detector, as well as the detector assembly and connection were performed. First test measurements with the Ost detector in the TOF-mode have been carried out and demonstrated the performance capability of all detector elements and the need for its further adjustment (selection of operating voltage, detection thresholds, etc.).

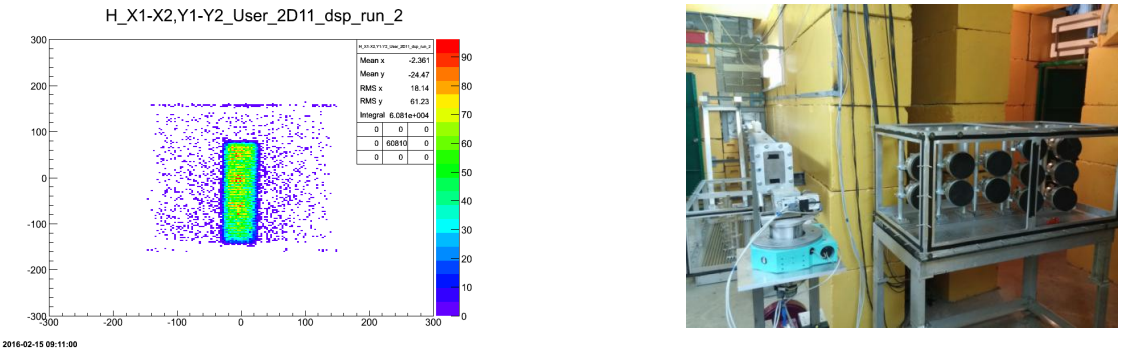

(a) (b)

***Fig. 1-I-26**. Neutron intensity distribution at the exit of the FSS mirror neutron guide measured by PSD detector (a). Detector Ost (without shielding) after installation and alignment of 12 PMTs with glued ^{6}Li glasses. At the sample position, modules of the HUBER goniometer are installed and adapted to the FSS table (b).*

On the REMUR reflectometer, a spectral width of the microbeam emitted from the end of a flat waveguide has been investigated as a function of the angular divergence of the incident beam, **Fig. 1-I-27** [30].

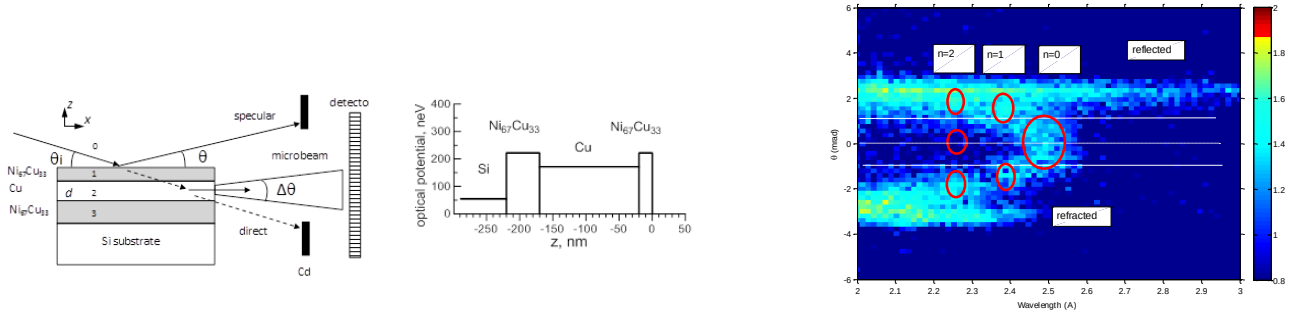

(a) (b) (c)

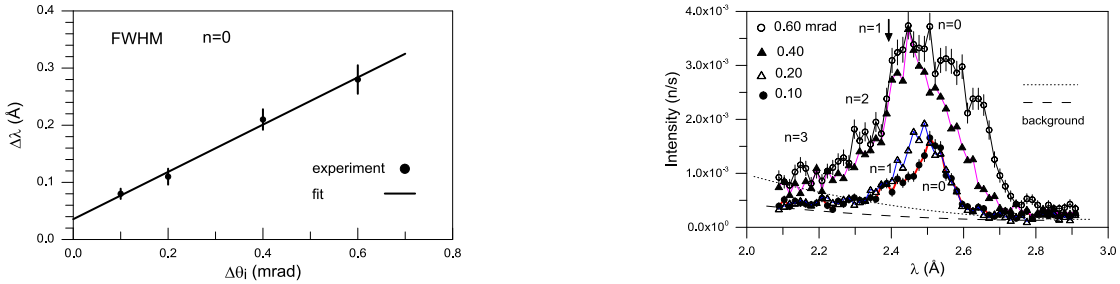

(d) (e)

***Fig. 1-I-27**. Scheme of experiment (a). Neutron optical potential of sample depending on z-coordinate perpendicular to sample layers (b). 2D-dimensional neutron counting map depending on wavelength and scattering angle at fixed grazing angle of incident beam of 3.69 mrad. Ellipses show the maxima of transmitted microbeams for resonances of orders n = 0, 1, 2 (one, two and three maxima over scattering angle, respectively) (c). Microbeam wavelength resolution for resonance order n = 0 and its dependence on angular divergence of incident beam (points - experiment, vertical dashes - experimental errors). Solid line shows linear fit (d). Integral microbeam intensity around sample horizon depending on neutron wavelength at different angular divergence of incident beam: 0.60, 0.40, 0.20 and 0.10 mrad. Marked peaks correspond to resonance orders n = 0, 1, 2, 3 (e).*

It has been shown that the spectral width of the microbeam decreases with diminishing angular divergence of the incident beam. By extrapolating the linear dependence in the zero divergence point of the initial beam and subtracting the reactor pulse duration, the spectral width of the resonance has been experimentally evaluated. The agreement of this value with the theoretical estimate testifies that the description of the resonance properties of the waveguide system is correct. The knowledge of the spectral width of the microbeam makes it possible to evaluate the wavelength resolution limit by probe microscopy. This method uses the Larmor precession of the spin of neutrons in the microbeam passing through the sample and scanning it with a high spatial resolution.

The study of the operating modes of the spin-echo small-angle (SESANS) spectrometer with linearly increasing magnetic fields which is under construction at beamline 9 of IBR-2, has been continued using Monte Carlo simulations (VITESS software package) with the parameters: distance between spin rotators in each arm – 60 cm, thickness of spin rotators a = 2 cm, period of sawtooth pulses T = 1 ms, pulse amplitude B = 500 Oe, inclination of spin rotators relative to the instrument axis $\alpha = 60°$. The TOF spectrum had the wavelength range of 1-15 Å, and the polarization of the beam before entering the first arm of the setup was directed along the Z-axis and was 100% in the entire wavelength range. The scattering object was a set of homogeneous monodisperse spheres. To determine the working intervals in the spectrum $\Delta\lambda$ meeting the necessary criteria, the simulation of the polarization as a function of neutron wavelength $P_z(\lambda)$ was carried out in the absence of the sample. The working plateaus with the length $\Delta\lambda$ covering about 10 time-of-flight channels with 64 ms width are narrow but sufficient for measurements. To simulate the scattering curves, neutrons with wavelengths from the plateaus were used. Neutrons from different working intervals form different scattering curves corresponding to different operation modes of the instrument *n* (**Fig. 1-I-28**). The results of the simulation of the SESANS experiment in the VITESS package fully coincide with the analytical calculations, which confirms the correctness of the virtual instrument. This result means that the obtaining of data on the object under study in the considered method is related to the necessity to separately consider different parts of the scattering curves obtained in one measurement. Further technical development of the technique based on the possibility of the broadening of the field pulses under a constant time gradient can reduce the number of modes to two or even one. It is clear that this development will require more powerful power supplies and perfect cooling systems for the coils of spin rotators.

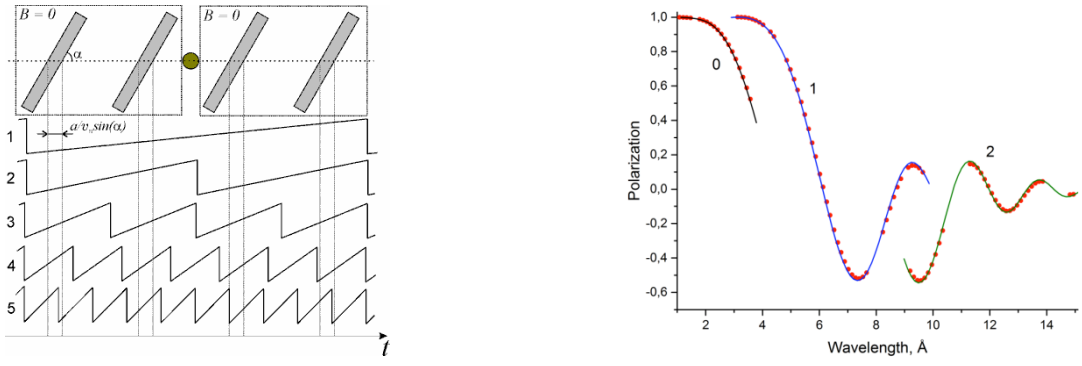

(a) (b)

***Fig. 1-I-28**. Time diagram for neutrons of different velocities: one sawtooth field pulse covers neutron time of flight through all four spin rotators (1); only two spin rotators (2); only one spin rotator (3); only one spin rotator and few pulses for time of flight between rotators (4); neutron hits a jump in magnetic field as it passes through at least one spin rotator (a). SESANS signal obtained for scattering from spheres with radius of 100 Å. Scattering curves clearly show formation of three different dependences corresponding to different modes of setup operation. Solid lines – analytical calculations (b).*

On the neutron radiography facility, a new two-mirror optical system of the detector has been designed to increase its radiation resistance (**Fig.1-I-29**). It has made it possible to reduce by several times the rate of radiation damages of the matrix in the CCD detector camera.

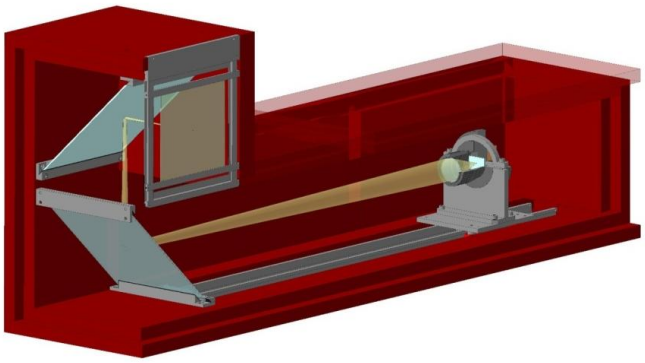

***Fig. 1-I-29**. Scheme of two-mirror optical system of the detector at the neutron radiography and tomography facility.*

On the YuMO instrument, a new unit for thermostating samples has been installed and tested. It has been shown that the use of the new unit increased the sample temperature range up to 120°C. It has been found that the temperature gradients are lower than expected. The number of simultaneously loaded samples has been extended to 25 samples.

References

[1] S.V.Ovsyannikov, M.Bykov, E.Bykova, D.P.Kozlenko, A.A.Tsirlin, A.E.Karkin, V.V.Shchennikov, S.E.Kichanov, H.Gou, A.M. Abakumov, R.Egoavil, J.Verbeeck, C.McCammon, V.Dyadkin, D.Chernyshov, S. van Smaalen, and L.S. Dubrovinsky “Charge ordering transition in iron oxide Fe_4O_5, involving competing dimer and trimer formation”, Nature Chemistry, v. 8, p. 501 (2016).

[2] N.T.Dang, D.P.Kozlenko, T.L.Phan, S.E.Kichanov, L.H.Khiem, S.H.Jabarov, T.A.Tran, N.V.Dang, T.D.Thanh, D.B.Vo, B.N.Savenko “Structural Polymorphism of Mn-Doped $BaTiO_3$” Journal of Electronic Materials, 45, 2477-2483 (2016).

[3] D.P.Kozlenko, N.T.Dang, T.L.Phan, S.E.Kichanov, N.V.Dang, T.D.Thanh, L.H.Khiem, S.H.Jabarov, T.A.Tran, T.V.Manh, A.T.Le, B.N.Savenko “The Structural, Magnetic and Vibrational Properties of Ti-doped $BaMnO_3$” Journal of Alloys and Compounds, accepted (2016).

[4] A.M.Balagurov, I.A.Bobrikov, S.V.Sumnikov, V.Yu.Yushankhai, N.Mironova-Ulmane, Magnetostructural phase transitions in NiO and MnO: Neutron diffraction data, JETP Lett. 104 (2016) 88 - 93

[5] S.Ya.Istomin, V.V.Chernova, E.V.Antipov, M.V.Lobanov, I.A.Bobrikov, V.Yu.Yushankhai, A.M.Balagurov, K.Y.Hsu, J.-Y.Lin, J.M.Chen, J.F.Lee, O.S.Volkova, A.N.Vasiliev “Wide range tuning of Mo oxidation state in $La_{1-x}Sr_xFe_{2/3}Mo_{1/3}O_3$ perovskites” European Journal of Inorganic Chemistry, v. 2016 (18), pp. 2942–2951 (2016).

[6] A.M.Balagurov, I.A.Bobrikov, B.Mukhametuly, S.V.Sumnikov, I.S.Golovin, Coherent cluster atomic ordering in the Fe-27Al intermetallic compound, JETP Lett. 104 (2016) 539–545.

[7] M.Kubovcikova, Gapon I.V., Zavisova V., Koneracka M., Petrenko V.I., Soltwedel O., Almasy L., Avdeev M.V., Kopcansky P. On the adsorption properties of magnetic fluids: impact of bulk structure. JMMM, 2016, in press.

[8] A.V.Nagornyi, Petrenko V.I., Avdeev M.V., Yelenich O.V., Solopan S.O., Belous A.G., Gruzinov A.Yu., Ivankov O.I., Bulavin L.A. Structural aspects of magnetic fluid stabilization in aqueous agarose solutions. JMMM, 2016, in press.

[9] J.Majorosova, V.I.Petrenko, Siposova K., Timko M., Tomasovicova N., Garamus V.M., Koralewski M., Avdeev M.V., Leszczynski B., Jurga S., Gazova Z., Hayryan Sh.,Hu Chin-Kun, Kopcansky P. On the adsorption of magnetite nanoparticles on lysozyme amyloid fibrils. Colloids Surf. B, 2016, V. 146, pp. 794–800.

[10] V.Gdovinova, Tomasovicova N., Batko I., Batkova M., Balejcikova L., Garamus V.M., Petrenko V.I.,

1. SCIENTIFIC RESEARCH

Avdeev M.V., Kopcansky P. Interaction of magnetic nanoparticles with lysozyme amyloid fibrils. JMMM, 2016, in press.
[11] Petrenko V.I., Avdeev M.V., Bulavin L.A., Almasy L., Grigoryeva N.A., Aksenov V.L. Effect of surfactants excess on the stability of low-polarity ferrofluids probed by small-angle neutron scattering. Crystallography reports, 2016, V. 61, Issue 1, pp. 121-125
[12] Yu.I.Prylutskyy, Cherepanov V.V., Kostjukov V.V., Evstigneev M.P., Kyzyma O.A., Bulavin L.A., Ivankov O., Davidenko N.A. and Ritter U. Study of the complexation between Landomycin A and C60 fullerene in aqueous solution. RSC Adv., 2016, V. 6, pp. 81231-81236.
[13] S.Prylutska, Panchuk R., Gołuński G., Skivka L., Prylutskyy Yu., Hurmach V., Skorokhyd N., Borowik A., Woziwodzka A., Piosik J., Kyzyma O., Haramus V., Bulavin L., Evstigneev M., Buchelnikov A., Stoika R., Berger W., Ritter U., Scharff P. C60 fullerene enhances cisplatin anticancer activity and overcomes tumor cells drug resistance. Nano Res., 2016, accepted.
[14] M.V.Avdeev, Tomchuk O.V., Ivankov O.I., Alexenskii A.E., Dideikin A.T., Vul' A.Ya. On the structure of concentrated detonation nanodiamond hydrosols with a positive ζ potential: analysis of small-angle neutron scattering. Chemical Physics Letters, 2016, V. 658, P. 58-62.
[15] M.V.Avdeev, Rulev A.A., Bodnarchuk V.I., Ushakova E.E., Petrenko V.I., Gapon I.V., Tomchuk O.V., Matveev V.A., Pleshanov N.K., Kataev E.Yu., Yashina L.V., Itkis D.M. Monitoring of Lithium Plating by Neutron Reflectometry. Applied Surface Science, 2016, accepted.
[16] I.M.Byvshev, Vangeli, I. M., Murugova, T. N., Ivankov, O. O., Kuklin, A. I., Popov, V. I., Yaguzhinsky, L. S. On the existence of two states of OXPHOS system supercomplex in heart mitochondria. Biochimica et Biophysica Acta - Bioenergetics, 1857, e35-e36 (2016).
[17] M.Zhernenkov, D.Bolmatov, D.Soloviov, K.Zhernenkov, B.P.Toperverg, A.Cunsolo, A.Bosak & Y.Q.Cai. Revealing the mechanism of passive transport in lipid bilayers via phonon-mediated nanometre-scale density fluctuations. Nature Communications, 7, 1-9 (2016).
[18] D.Lombardo, P.Calandra, D.Barreca, S.Magazu, M.A.Kiselev. Soft Interaction in Liposome Nanocarriers for Therapeutic Drug Delivery. Nanomaterials 6, 125 (2016).
[19] N.Kučerka, Dushanov E., Kholmurodov Kh., Katsaras J., Uhríková D. Cation-containing lipid membranes – experiment and MD simulations. European Pharmaceutical Journal, 2016, accepted.
[20] M.Ordon, Yu.Gorshkova, M.Ossowska-Chruściel. Lithocholic acid derivative in the dimethyl sulfoxide presence: Morphology and phase transitions, Thermochimica Acta 643 (2016) 1–12.
[21] Y.V.Kulvelis, et al., Structure and properties optimization of perfluorinated short side chain membranes for hydrogen fuel cells using orientation stretching. RSC Advances, 6, 108864–108875 (2016).
[22] L.Bulavin, Kutsevol, N., Chumachenko, V., Soloviov, D., Kuklin, A., & Marynin, A. (2016). SAXS Combined with UV-vis Spectroscopy and QELS: Accurate Characterization of Silver Sols Synthesized in Polymer Matrices. Nanoscale research letters, 11(1), 1-8 (2016).
[23] T.V.Tropin, J.W.P.Schmelzer, V.L.Aksenov. Modern aspects of the kinetic theory of glass transition. Physics – Uspekhi, 59 (1) pp.42-66 (2016).
[24] Ł.Hetmańczyk, D.Chudoba, A.Filarowski et al. To the question of conformational equilibrium and polymorph's states in the solid state and under the matrix condition. J. Chem. Phys., submitted (2016).
[25] R.Keppler, Stipp, M., Behrmann, J.H., Ullemeyer, K. & Heidelbach, F. Deformation inside a paleosubduction channel – Insights from microstructures and crystallographic preferred orientations of eclogites and metasediments from the Tauern Window, Austria. J. Struct. Geol. 82, 60-79 (2016).
[26] T.Lychagina, & Nikolayev, D. Quantitative comparison of the measured crystallographic textures. J. Appl. Cryst. 49 (4), 1290-1299 (2016).
[27] D.Nikolayev, & Lychagina, T., Zisman, A.A. & Yashina, E. Directly verifiable neutron diffraction technique to determine retained austenite in steel. Materials Science and Engineering A., submitted (2016).
[28] Ch.Scheffzük, Müller, B.I.R., Breuer, S., Altangerel B. & Schilling, F.R. Applied Strain Investigation on Sandstone Samples Using Neutron Time-of-Flight Diffraction at the Strain Diffractometer EPSILON, IBR-2M Dubna. Mongolian J. Physics, submitted (2016).
[29] S.Breuer, Schilling, F.R., Scheffzük, Ch. & Müller, B.I.R. Forward Modeling Neutron Time-of-Flight Diffraction Data for Uniaxial Load Conditions by Using the Example of Sandstone. J. Appl. Cryst., submitted (2016).
[30] S.V.Kozhevnikov, V.K.Ignatovich, F.Radu, Neutron resonances in planar waveguides, JETP, 123 (6) (2016) 950-956.